Article

Design, synthesis, and biological evaluation of itaconic acid derivatives as potential anti-influenza agents

Bidyadhar Sethy, Chung-Fan Hsieh, Ta-Jen Lin, Po-Yuan Hu, Yu-Li Chen, Chia-Yi Lin, Sung-Nain Tseng, Jim-Tong Horng, and Pei-Wen Hsieh

J. Med. Chem., **Just Accepted Manuscript** • DOI: 10.1021/acs.jmedchem.8b01683 • Publication Date (Web): 12 Feb 2019

Design, synthesis, and biological evaluation of itaconic acid derivatives as potential anti-influenza agents

Bidyadhar Sethy[†], Chung-Fan Hsieh[‡], Ta-Jen Lin[‡], Po-Yuan Hu[‡], Yu-Li Chen[‡], Chia-Yi Lin[‡], Sung-Nain Tseng[§], Jim-Tong Horng[‡,§,∥,#,*], Pei-Wen Hsieh[†,⊥,#,∇,*]

[†]Graduate Institute of Biomedical Sciences, Division of Natural Products, College of Medicine, Chang Gung University, Taoyuan, 33302, Taiwan.

[‡]Department of Biochemistry and Molecular Biology, Chang Gung University, Taoyuan, 33302, Taiwan.

[§]Research Center for Emerging Viral Infections, Chang Gung University, Taoyuan, 33302, Taiwan.

[∥]Molecular Infectious Disease Research Center, Chang Gung Memorial Hospital, Chang Gung University, College of Medicine, Linkou, 333, Taiwan.

[⊥]Graduate Institute of Natural Products, School of Traditional Chinese Medicine, College of Medicine, Chang Gung University, Taoyuan, 33302, Taiwan.

[#]Research Center for Chinese Herbal Medicine, Chang Gung University of Science and Technology, Taoyuan, 33303, Taiwan.

[∇]Department of Anesthesiology, Chang Gung Memorial Hospital, Linkou, 333, Taiwan.

Abstract

Influenza A viruses (IAVs) have caused worldwide epidemics and pandemics by reassortment and generation of drug-resistant mutants, which renders antivirals and current vaccinations no longer usable. In this study, an itaconic acid derivative **1** was identified from a chemical library of 20,000 compounds by performing a cell-based screening assay as a lead agent exhibiting anti-influenza A activity. Accordingly, a series of itaconic acid derivatives were designed and synthesized by adopting a rational design strategy to obtain more potent anti-influenza agents. The results of an *in vitro* pharmacological study showed that compounds **4** and **8** exhibited the most potent anti-IAV effect with EC_{50} values of 0.14 and 0.11 μM, respectively, in Madin–Darby canine kidney cells. Mechanisms of action studies showed that lead agents **1** and **4** reduced virus replication by directly targeting IAV nucleoproteins and disrupting virus ribonucleoprotein export from nucleus to cytosol. On the basis of its high potential as an anti-IAV agent and its selectivity index > 785, compound **4** was found to be a promising candidate for further development against IAVs.

Keywords: Anti-influenza A; drug discovery; itaconic acid derivatives; Michael-acceptor moiety; nuclear export inhibitor.

INTRODUCTION

Influenza A virus (IAV) is a negative-sense single-stranded RNA virus that belongs to the family of *Orthomyxoviridae*. IAV is the most virulent human pathogen and causes severe diseases, with infants, elderly people, pregnant women, and people with weakened immune systems at high risk.[1] The symptoms of influenza virus infections include fever, muscle aches, headaches, vomiting, and diarrhea and influenza may cause pneumonia, myocarditis, encephalitis, or myositis, and sometimes even death.[2] In the past century, five notorious influenza pandemics occurred, which not only caused >45 million human deaths but also resulted in stupendous economic losses due to their high rates of morbidity and mortality.[3-6] Currently, H1N1, H3N2, H5N1, and H7N9 subtypes of influenza A are highly aggressive seasonal flu strains that circulate in human populations and are a significant threat to human health.[7,8] To overcome these pathogens and other emerging mutants, development of unique therapeutic strategies or drugs is urgently needed.[7-11]

To prevent or reduce the influenza A virus infections, vaccination is generally recommended.[12-14] For influenza therapy, two classes of antiviral drugs have been clinically used: virion ion-channel (M2 protein) inhibitors (amantadine and rimantadine) and neuraminidase (NA) inhibitors (oseltamivir and zanamivir). However, IAVs have developed resistance to these anti-influenza agents.[6,15-18] Consequently, there is an urgent need to develop agents with different mechanisms of action on viral life cycles.

Since influenza viruses replicate, transcript, and generate viral proteins, such as virus ribonucleoproteins (vRNPs) in the nuclei of infected cells, and then transport them to the cytoplasm, transfer of nuclear viral materials is a critical step in the influenza virus life cycle.[19,20] In this step, the well-known host chromosomal region maintenance 1 (CRM1; also referred to as Exportin 1 or XPO1) can interact with nuclear export signal (NES)-containing viral nuclear export proteins, which are then exported to the cytoplasm.[21-24] This CRM1 is an important protein involved in the nuclear export process that regulates cell proliferation, cell-cycle progression, and apoptosis and is related to many diseases, such as cancer and viral infection.[20,21,25,26] Accordingly, development of nuclear export inhibitors (NEIs) to block this pathway could be useful to provide a new therapeutic strategy against influenza.[19,20]

In an effort to explore new lead compounds for anti-influenza A agents, large-scale screening of a chemical library containing > 20,000 compounds against IAV was performed by using a cell-based anti-cytopathic effect (CPE) assay. Our first hit was *N,N′*-bis(2,4-difluorophenyl)-2-methylenesuccinamide (**1**, **Figure 1**), an itaconic acid derivative that exhibited anti-influenza activity with a half-maximal effective concentration (EC_{50}) of 2.84 μM. This compound is the first itaconic acid derivative to show anti-influenza activity. We then synthesized 25 itaconic acid derivatives, and their effects against IAV were evaluated. Subsequently, structure–activity relationships (SARs) were established. Furthermore, since the chemical structure of **1** bears a Michael-acceptor moiety, which is a privileged structure for NEIs,[21] the mechanism of action of **1** against IAV was examined.

RESULTS AND DISCUSSION

The chemical structure of **1** consists of two 2,4-di-fluoro-phenyl moieties (Units A and B, **Figure 1**) and an itaconic acid moiety (Unit C, **Figure 1**), which are linked together by two amide bonds. Previous literature reports concluded that Unit C of **1** has a conjugated system that is able to react with the cysteine residue of the active site through Michael addition.[21] Therefore, to discuss the correlation between the reactivity of the conjugated system in **1** toward the active site and its bioactivities, Units A and B were modified by varying their aromatic substituents. Using an addition/elimination reaction mechanism, a one-step synthetic route was developed (**Scheme 1**), which led to 25 itaconic acid derivatives. The purities of all compounds (>96%) were evaluated by high-performance liquid chromatography (HPLC) (**Suppl. Table S1** and **S2**). Furthermore, the anti-IAV effects and cytotoxicities of these compounds were determined in an influenza A (A/WSN/33) virus-infected Madin–Darby canine kidney epithelial (MDCK) cells model.

SARs based on anti-IAV (H1N1) activity

To evaluate the antiviral activity and cytotoxicity of the itaconic acid derivatives, a CPE assay and an MTT assay were performed in parallel (**Table 1 & 2**). Two nuclear export inhibitors, leptomycin B (LMB) and verdinexor, were used as positive controls. The cytotoxic results (50% cytotoxic concentration, CC_{50}) indicated that, except for compounds **1**, and **6-8**, most of the derivatives were non-cytotoxic at 110 μM. Compounds **4**, **7**, **8**, and **9** exhibited the most potent effects on anti-IAV, with EC_{50} values of 0.14, 0.18, 0.11, and 0.48 μM, respectively. The selectivity indices (SIs) of **4** and **9** were better than that of verdinexor, indicating that **4** and **9** could be good candidates against IAV. The SARs of the synthetics are discussed below on the basis of their antiviral activities.

Initially, we modified the *para* (*p)* position of the two aromatic rings (Units A and B) of the lead agent **1** by introducing different electron-withdrawing groups (EWG) such as Cl, Br, or trifluoromethyl (–CF_3), or an electron-donating group (EDG). The results showed that when *p*-F (**1**) was replaced with *p*-Cl (**2**), *p*-Br (**3**), or *p*-CF_3 (**4**) the antiviral activities were significantly improved by the presence of lipophilic (halo) groups, with an electron-withdrawing property at the *para* position. Subsequently, to gain a better understanding of the electronic property at the *p*-position, we introduced a methoxy group (-OCH_3), which resulted in reduced activity. From these results, we concluded that the presence of a highly EWG (-CF_3) at the *p*-position (Units A and B) improved the activity while decreasing the cytotoxicity. These effects were most likely caused by the presence of the strong EWG at the *p*-position facilitating a Michael-type addition and favoring the lipophilic interaction with the active core, which would increase the inhibitory property with high SIs. Accordingly, we concluded that EWG substitution, compared with EDG substitution, at the *p*-position improved antiviral activity.

We observed that moving the fluoro-group of Units A and B from the *para* to the *meta* position (**6**) slightly enhanced antiviral activity but led to increased cytotoxicity. Similarly, replacing *m*-F (**6**) with *m*-Cl (**7**) or *m*-CF_3 (**8**) not only improved potency but also triggered cytotoxicity (**Table 1**). We also found that the compounds containing a *p*- or *m*-trifluoromethyl group (**4** and **8**) exhibited 20–25-fold higher anti-IAV activity (**Table 1**). Since the Cys-539 residue is a prime target located within the hydrophobic nuclear export sequences-binding region of CRM1, the hydrophobic trifluoromethyl group may occupy the hydrophobic groove, being buried deeply into the active site, thereby promoting antiviral activity.[27] To test our hypothesis, we performed

molecular docking of compounds **4** and **8** in the active sites of LMB in CRM1 (PDB ID: 4HAT). The results showed that the Michael-acceptor moiety (Unit C) of **4** and **8** (**Figures 2A & 2B**), and the LMB lactone (**Figure 2C**) were closely fit at the active residue (Cys-539). Moreover, a comparison of the docking poses of **4** (purple) and **8** (green) with the binding site of LMB (blue) showed that an aromatic ring conjugated with the hydrophobic trifluoromethyl group of compounds **4** and **8** was located in the hydrophobic groove of the LMB binding sites of CRM1 (**Figure 2D**). Notably, **4** bound to the active site by hydrogen bonding with the Lys-579 residue and **8** interacted with Lys-548 through hydrogen bonding, and the presence of Cys-539 helped preserve their activities. Conversely, introducing an EDG, such as the methoxy (-OCH_3) group (**9**), promoted antiviral activity with lower cytotoxicity (**Table 1**). Comparison of the data of **9** and **5** showed that the strong effect of a donating group at the *meta* position on the electron density of the aromatic ring may concomitantly improve efficiency against IAV.

Next, to examine the effect of the substitution at the *ortho* position, the F group in **1** was replaced with Br (**10**), which led to relatively similar activity and slightly reduced cytotoxicity (**Table 1**). However, the antiviral activities completely vanished after introducing a CF_3 group in the *o*-position (**11** and **12**) (**Table 1**). These results indicated that the presence of a strong EWG at the *o*-position had a negative effect on activity. Moreover, two analogs (**1** and **6**) containing both *m*- and *p*-F substitutions along with *o*-F on each aromatic ring exerted an inhibitory effect against IAV, most likely because of the hydrophobic property of the F group promoting formation of pi-alkyl hydrophobic interactions with the active site (**Suppl. Figure S51A and S51B**), which would lead to activity retention.

Extending the carbon chain between the amides and aromatic rings inhibited the effect against IAV (**Table 1**), which suggested that **14** and **15** are unable to fit the active site. Furthermore, the presence of a lone electron pair on the amide nitrogen atom may disturb the conjugate system present on **14** (**Figure 3A**) or **15** by direct conjugation with the carbonyl carbon. This contrasts with the case of **1** (**Figure 3B**) in which direct conjugation with the Michael-acceptor moiety was hindered by the withdrawal property of the EWG, which resulted in a resonance effect on the nitrogen lone pair that is drawn toward the benzene ring.

It was previously reported that the high electronegativity of fluorine substitution can enhance potency and affect target selectivity by affecting pK_a, lipophilicity, hydrophobic interactions, and drug metabolism. In addition, a fluoro atom at the *o*-position interacts with the amide proton (N–H), thereby leading to improved permeability.[28] In synthetics possessing an F group at the *o*-position, the interaction with N–H by intramolecular hydrogen bonding could have an effect on antiviral activity. Accordingly, ^{1}H-NMR data showed that the NH signals were downfield shifted when an *o*-F group was present on the aromatic ring (Units A and B).[29] The presence of different substituents (EWG or EDG) on the aromatic ring counterbalanced the electron-withdrawing effect of the *o*-F group by a resonance effect, which preserved the intramolecular hydrogen bonding and anti-IAV activity. However, in systems containing CF_3 where π-resonance is not possible, the inductive electron-withdrawing effect of fluorine could exert a powerful influence on *o*-substituents and increase the chemical shift of the NH signals. On the other hand, extending the carbon chain between the amide proton and aromatic ring could disrupt the conjugating system and the N-H–F interaction, which might contribute to the reduced activity in **14** and **15**

(**Table 1**). This idea suggests that intermolecular hydrogen bonding might also enhance the anti-IAV activities of these analogs.

To further investigate the activity of Unit A, we synthesized 10 derivatives (**1A–10A**) of itaconic acid by conjugating the aromatic ring only at the Unit A side and evaluated their anti-influenza A activity. Additionally, the chemical structures of this series were confirmed by 2D NOESY spectra. According to the results summarized in **Table 2**, all of these products were non-active, which indicated that the presence of two aromatic rings (Units A and B) is necessary for anti-influenza activity.

Since the two aromatic rings containing derivatives have similar structures, we initially selected lead agent **1** to examine its effectiveness against different strains of influenza virus and other viruses as well as to study the stage of action on influenza A virus.

Antiviral activity of compounds 1 & 4 on various strains of viruses

To evaluate the effectiveness of the itaconic acid analogues (**1** and **4**) against various strains of viruses, we chose some strains especially those are clinically resistant to the drug Oseltamivir (A/TW/7855/09 and A/TW/6663/09) and Swine Origin Influenza Virus (SOIV) strain caused pandemic (A/TW/90206/09 and A/TW/2235/09) in last decade and also others those are endemic in Taiwan in recent years. Cytotoxicity tests using **1** & **4** were conducted in different cell lines, and the results were expressed as the median cytotoxic concentration (CC_{50}). The half-maximal effective concentration (EC_{50}) was used to express the inhibitory effects of **1** & **4** on different virus strains. Both of these compounds can effectively inhibit the replication of influenza virus in

MDCK cells with high CC_{50} values. The inhibitory effect of **1** was satisfactory on many IAV strains, such as A/WSN/33 (H1N1), A/TW/90206/09 (H1N1pdm), A/TW/2235/09 (H1N1pdm), A/TW/7855/09 (H1N1), A/TW/6663/09 (H1N1), and A/TW/3446/02 (H3N2), with EC_{50} values of approximately 2–5 μM (**Table 3**). It is worth noting that the A/TW/7855/09 (H1N1) and A/TW/6663/09 (H1N1) strains are resistant to the drug oseltamivir, which suggests that **1** could exert a therapeutic effect on virus strains that show resistance to oseltamivir. In addition, **1** exhibited a good inhibitory effect on the influenza B virus strains popular in recent years, including B/TW/00482/13, B/TW/03384/13, B/TW/00642/14, and B/TW/01061/14, with EC_{50} values between 3 and 4 μM (**Table 3**) and greater SIs (>18). Further, the anti-influenza effect of **4** gave a five- to eight-fold higher activity for A/WSN/33 (H1N1) and A/TW/3446/02 (H3N2) strains and slightly improved activity for A/TW/2235/09 (H1N1pdm) than those of compound **1** with higher SI values. Compounds **1** & **4** also had inhibitory effects on enterovirus A71, with an EC_{50} value of approximately 4–7 μM, whereas it had no inhibitory effect on either enterovirus D68 or rhinovirus, which are evaluated by using rhabdomyosarcoma (RD) cells. Although the influenza virus has high variability, this does not affect the inhibitory effect of **1** on different strains of influenza A and B type along with **4** on influenza A viruses. Thus, **1** & **4** show an extensive spectrum of inhibition against influenza viruses, drug-resistant strains, and enterovirus A71.

Microscopic observation of IAV-induced cytopathic effect inhibition by 1.

Virus-induced cytopathic changes were examined in MDCK cells, which were infected with influenza virus A/WSN/33 with a multiplicity of infection (MOI) of 0.5 for 1 h, washed with phosphate-buffered saline (PBS), then treated with **1** (10 μM) and observed under a microscope

post infection (pi) = 12 or 36 h (**Figure 4**). We found that the influenza virus caused some cytopathic changes after 12 h and serious cytopathic effects with more round-up cells after 36 h in the virus-only group. When co-treating drugs and viruses, we found that **1** could avoid cytopathic phenomena caused by viral infection after 36 h, and the infection did not spread through surrounding cells (**Figure 4**). With regard to toxicity, no cytotoxic effect caused by **1** was observed after 36 h. It seems reasonable to conclude that **1** has very low or no toxicity to MDCK cells.

Mechanism of action study: estimation of the inhibition period of 1 in A/WSN/33 by using time-course test.

The influenza virus life replication/cycle occurs in multiple steps, which requires approximately 8–10 h to complete.[30] For the time-of-addition (TOA) assay, the following main steps are to be considered: virus attachment, entry, uncoating, translation, replication, and release. In this study, we performed a TOA experiment by using MDCK cells infected with A/WSN/33 (multiplicity of infection, MOI = 0.1) and treated with 10 μM of **1**. We designed this experiment according to the indicated time points for drug treatments, and the virus was allowed to absorb at −1 to 0 h pi. The supernatant was collected after 9 h for a plaque assay (**Figure 5A**). To examine whether compound **1** targets host cell factor, the drug was treated 2 h prior to virus infection (−3 to 9 h pi; complete cycle). The periods indicate virus attachment, and then virus entry or uncoating (−1 to 9 h and 0 to 9 h pi, respectively), the middle stage of virus cycle endocytosis, translation, replication (3 to 9 h pi), and finally the assembly and release of progeny virus (6 to 9 h pi). From the TOA experiment, we found that **1** mainly inhibited the virus during the early and middle stage of replication, whereas it was less effective at the late stage relative to that in the virus only

lane (**Figure 5B**). To verify the actual stage of inhibition, the following experiments, i.e., hemagglutinin inhibition (HAI) assay, viral RNA synthesis, and viral protein distribution test by immunofluorescence staining, were performed.

Effect of hemagglutinin (HA) activity in A/WSN/33 virus upon treatment with 1

In the early stage of viral replication, the virus attaches to the host cells by their surface glycoprotein HA. From the TOA experiment, we found that **1** inhibited early steps of virus replication. Therefore, we used the HAI assay to verify whether **1** blocked the early virus attachment by inhibiting the hemagglutination of red blood cells (RBCs) caused by viral HA protein. When the viral protein HA was used to contact the receptor on the surface of RBCs, hemagglutination was generated to detect whether the drug inhibited HA activity. RBCs were treated with various concentrations of **1** (two-fold serial dilution from 50 μM) and incubated with influenza A/WSN/33 at 4 × HA on ice for 1 h. The results showed that **1** alone (upper row, **Figure 6**) was not able to form agglutination similar to that of RBCs only (Mock, lane 12), and virus treated with **1** could not inhibit the hemagglutination caused by viral HA (lower row, **Figure 6**). Therefore, this result indicated that **1** did not inhibit the activity of HA, and there was no significant correlation between **1** and influenza virus attachment and entry into cells.

Compound 1 did not interrupt viral RNA and protein synthesis

According to time-course experiments, **1** also inhibited the middle stages of viral replication; therefore, it was necessary to investigate whether **1** inhibits viral RNA and protein synthesis. After infecting MDCK cells with influenza virus (MOI = 0.1) for 1 hour, **1** was added, and cell lysates were collected at pi = 3, 6, and 9 h for RNA and protein determination by reverse

transcription-quantitative polymerase chain reaction (RT-qPCR) and immunoblotting assay (**Figure 7A**). From the RT-qPCR results depicted in **Figure 7B**, it can be seen that no significant increase in viral RNA synthesis occurred at 0–3 h pi, whereas they showed an exponential rise at 3–9 h pi. The M1 RNA levels indicated that **1** did not inhibit viral RNA synthesis. Additionally, the effect of **1** on viral protein synthesis was examined by western blotting as indicated by the level of various viral proteins (**Figure 7C**). The results implied that **1** did not inhibit the biosynthesis of viral proteins (NP, M1, HA, PA, NS2, and NS1). Thus, we confirmed that **1** did not inhibit viral RNA and protein expression.

Effect of 1 on the subcellular distribution of viral proteins

We used immunofluorescence staining to detect the location of viral proteins in the cells to examine whether **1** affected their distribution. Thus, the effect of **1** was evaluated by using MDCK cells, which were infected with influenza virus A/WSN/33 (MOI = 0.1), and the infected cells were treated with DMSO (mock; 0.05%) or **1** (10 μM), or leptomycin B (LMB; 10 nM) as control group. Then, the cells were fixed after 9 h pi and stained using the specific antibodies. From the results of IF staining, it can be seen that NP (**Figures 8A** & **8B**) was transported into the cytoplasm in case of influenza virus infection, but after **1** or LMB treatment, the NP of the influenza virus was confined to the nucleus. In contrast, the viral proteins NS2 (**Suppl. Figure S52A**), PA (**Suppl. Figure S52B**), and M1 (**Suppl. Figure S52C**) did not exhibit significant differences in their nucleus/cytosol distribution after treatment with **1** or LMB compared with the virus-only control (**Suppl. Figure S52D**). Notably, LMB is an NEI that acts as an antiviral and anticancer agent, and its main function is to block the cargo/exportin transport from the nucleus to cytoplasm by targeting the host cellular CRM1 protein. During the viral infection, the CRM1

protein helps to localize viral proteins in appropriate positions and interrupts the cellular cargoes. LMB efficiently binds the receptor sites of CRM1, resulting in inhibition of nuclear export of viral NP by disturbing the nuclear export signal 3-dependent CRM1 binding. In addition, as can be extracted from the literature, LMB has been shown to inhibit vRNP export while not affecting the subcellular localization of other viral proteins, such as matrix protein 1 (M1) and non-structural protein 2 (NS2).[31] As we hypothesized, **1** gave rise to a similar phenomenon (such as NEI). The IF staining result indicated that **1** specifically inhibited the nuclear export of viral NP, and PA also exhibited a different pattern in the presence of **1** because it surrounds the nucleus, thereby preventing its release into the cytoplasm, but the subcellular distribution of M1 and NS2 proteins is not affected.

In addition, the mechanism of action for compound **4**, which has the highest SI among all itaconic acid derivatives presented here, was also investigated by performing the TOA assay, HAI assay, and indirect immunofluorescence assay. TOA data indicated that **4** (1 μM) efficiently inhibited the virus in the early and middle stage of replication, similar to **1** (10 μM) (**Suppl. Figure S53**). Furthermore, **4** also did not inhibit the hemagglutination caused by viral HA, which suggested that **4** does not inhibit the virus attachment (**Suppl. Figure S54**). Finally, the immunofluorescence data revealed that the **4**-treated group showed inhibition of the middle stage of virus replication by specifically blocking subcellular distribution of viral NP to cytosol (**Figure 9**), without affecting other viral proteins, such as M1 (**Suppl. Figure S55**). Since these phenomena are similar to those of treatment with LMB and **1**, it appears that the mechanism underlying the activity of **4** is similar to that underlying **1**.

CONCLUSION

With the aim of developing a new class of anti-influenza agents, we designed and synthesized 25 itaconic acid derivatives based on the chemical structure of lead agent **1**, and their activities against IAV were evaluated in MDCK cells. The corresponding SARs of the derivatives were also proposed according to the bioactivity results. Activity and cytotoxicity improved after substitution with a highly EWG with larger size at the *p*-position of the aromatic rings. In contrast, the presence of an EDG at the *m*-position lowered cytotoxicity. Bulky groups at the *o*-position also caused a decrease in activity. Additionally, the presence of two aromatic rings bonded to itaconic acid was crucial for activity retention. Among all compounds tested, **4** showed excellent activity (EC_{50} = 0.14 μM), with a high SI (>785). Further, the initial hit agent **1** and its derivative **4** showed a broad spectrum of inhibition on different influenza strains along with enterovirus A71 viruses. A preliminary mechanism study using the lead agents **1** and **4** was conducted and showed that reduction of virus replication was caused by disruption of viral NP export from the nucleus to the cytoplasm. This finding suggests that viral NP may be a possible molecular target for these agents as NEIs, which presents a new opportunity for antiviral drug development. Therefore, **4** and its active derivatives are promising anti-influenza agents that should be further investigated in more detail.

EXPERIMENTAL SECTION

Chemistry: materials and methods

All of the chemical reagents and solvents were purchased from the commercial suppliers and used without further purification unless stated otherwise. Thin-layer chromatography (TLC; silica gel 60 F254 HX244089, Merck KGaA, Darmstadt, Germany) was used to monitor the

chemical reactions, and the TLC plates were read under ultraviolet (UV) light (Entela® UVGL-25 254/365 nm; CA, USA). Compounds were purified by flash column chromatography on silica gel (SiliaFlash® G60, 70–230 mesh and Siliaflash P60, 230–400 mesh, Silicycle, QC, Canada). A Bruker AVANCE-400 MHz FT-NMR (Karlsruhe, Germany) instrument was used to measure ^{1}H and ^{13}C NMR spectra at 400 MHz and 100 MHz, respectively. Deuterated solvents ($CDCl_3$ and acetone-d6) were used to calibrate the peaks, and trimethylsilane was used as internal standard for $CDCl_3$. Mass spectra were measured on a TSQ quantum triple quadruple mass spectrometer, Thermo Finnigan, CA, USA. A Hitachi U-2010 spectrophotometer (Tokyo, Japan) was used to record UV spectra, and a JASCO FT/IR-4100 spectrophotometer (Tokyo, Japan) was used to measure infrared spectra of all title compounds. Melting points were measured by using a MEL-TEMP® (Laboratory Devices, Inc., MA, USA) apparatus. A rotary vacuum evaporator (N-1100; EYELA, Tokyo, Japan) was used for removal of solvents. HPLC purity analyses were conducted by using a JASCO system: UV–VIS detector (UV-1575), autosampler (AS-1555–10), and pump (PU-1580), with UV detection at 230 nm, two different solvent systems (MeOH/H_2O and MeCN/H_2O), and a reversed-phase column (Necleodur C18 HTec EC250/4.65 μm, Macherey-Nagel, Duren, Germany). All target compounds had purities > 96% tested by HPLC.

Pan assay interference compounds (PAINS) analysis:

We examined all of the itaconic acid derivatives (1–15 and 1A–10A) for known classes of assay-interference compounds. First, according to the "Free ADME/Tox Filtering Tool 4 (FAF-Drugs4)" program (http://fafdrugs4.mti.univ-paris-diderot.fr/), compounds 1–15 and 1A–10A were not perceived as PAINS. The database "Aggregator Advisor" (http://advisor.bkslab.org/) showed that all of the synthetics were not aggregators. Further, all of the synthetics, neither as

aggregators and/or PAINS, were verified by using the Bulk Pattern Checker tool (http://zinc15.docking.org/patterns/home/). Thus, the activities provided herein are highly likely not to have been caused by pan assay interference.

General synthetic protocol for all title compounds (1–15) and (1A–10A)

To a solution of itaconyl chloride (1 equivalent) in anhydrous CH_2Cl_2 with molecular sieve at −4 to 0°C, halo-substituted aromatic aniline (2 equivalents) was added slowly by using a micropipette. The reaction mixture was stirred at −4 to 0°C for 1 h and then allowed to warm to room temperature for 4 h to 1 d. After confirming the completion of the reaction by TLC, the whole reaction mixture was filtered, and the filtrate was washed with CH_2Cl_2. The organic layer was quenched with a small volume of H_2O, the two layers were separated by using a separation funnel, and the organic layer was dried over Mg_2SO_4. Evaporation of the solvent afforded a mixture of expected products, along with some impurities, according to TLC. The mixture was purified by using silica gel column chromatography (hexane/ethyl acetate = 10/4) to obtain the desired products.

***N*,*N*'-bis(2,4-difluorophenyl)-2-methylenesuccinamide (1)**

Yield of 17.1% as white solid; mp (°C): 132-133; IR ν_{max} (KBr) cm^{-1}: 3385, 3247, 3232, 3090, 3028, 1665, 1616, 1518, 1430, 1263, 1223, 1143, 1098, 961, 853, 813, 628, 553, 490. UV λ_{max}^{MeOH} nm (Log Ɛ): 202.5 (4.5), 235.5 (4.1), 274.5 (3.8, sh); ^{1}H-NMR ($CDCl_3$, 400MHz) δ_H 8.73(1H, s, NH), 8.26-8.14 (3H, m, NH, H6′, and H6″), 6.93-6.82 (4H, m, H3′, H3″, H5′ and H5″), 5.99 (1H, s, H_b), 5.83 (1H, s, H_a), 3.49 (2H, s, H3); ^{13}C-NMR ($CDCl_3$, 100MHz) δ_C 168.4 (s, C4), 166.7 (s, C1), 159.3 (dd, *J*= 245.6, 11.5 Hz, C4′), 158.9 (dd, *J*= 244.7, 11.4 Hz, C4″),

153.3 (dd, *J*= 245.7, 11.7 Hz, C2′), 153.0 (dd, *J*= 246.1, 11.7 Hz, C2″), 138.6 (s, C2), 123.5 (t, C5), 123.4 (d, *J*= 9.1, Hz, C1′), 123.2 (d, *J*= 9.1 Hz, C1″), 122.8 (dd, *J*= 10.8, 10.8 Hz, C6′), 122.3 (dd, *J*= 10.2, 10.2 Hz, C6″), 111.5 (dd, *J*= 21.6, 3.7 Hz, C5′), 111.2 (dd, *J*= 21.5, 3.7 Hz, C5″), 103.9 (dd, *J*= 23.0, 23.1 Hz, C3′), 103.7 (dd, *J*= 23.1, 23.2 Hz, C3″), 41.5 (t, C3). ESI-MS (m/z): 375.2 $[M+Na]^+$.

4-((2,4-difluorophenyl)amino)-2-methylene-4-oxobutanoic acid (1A)

Yield of 13.3% as white solid; mp (°C): 170-171; IR ν_{max} (KBr) cm^{-1}: 3212, 3151, 3018, 2968, 2900, 1708, 1649, 1550, 1512, 1432, 1361, 1305, 1263, 1226, 1169, 1144, 1099, 968, 910, 859, 580, 485, 437; UV λ_{max} ^{MeOH} nm (Log Ɛ): 203.0 (4.4), 232.0 (4.1), 274.0 (3.3); ^{1}H-NMR (Acetone-*d6*, 400MHz) δ_H 8.99 (1H, s, NH), 8.19-8.12 (1H, m, H6′), 7.06 (1H, ddd, *J*= 8.8, 8.4, 2.8 Hz, H5′), 6.96 (1H, dd, *J*= 8.8, 8.4 Hz, H3′), 6.32 (1H, s, H_b), 5.86 (1H, s, H_a), 3.51 (2H, s, H3); ^{13}C-NMR (Acetone-*d6*, 100MHz)δ_C 169.4 (s, C1), 168.2 (s, C4), 159.5 (dd, *J*= 242.2, 11.3 Hz, C2′), 154.4 (dd, *J*= 245.4, 11.9 Hz, C4′), 136.3 (s, C2), 128.8 (t, C5), 124.4 (dd, *J*= 10.9, 3.4 Hz, C1′), 124.9 (d, *J*= 8.6 Hz, C6′), 111.7 (dd, *J*= 21.6, 3.6 Hz, C5′), 104.4 (dd, *J*= 23.7, 23.7 Hz, C3′), 40.8 (t, C3); ESI-MS (m/z): 239.9 $[M-H]^-$; HRMS calculated for $C_{11}H_8F_2NO_3$, $[M-H]^-$, 240.0467; found 240.0476.

***N*,*N*'-bis(4-chloro-2-fluorophenyl)-2-methylenesuccinamide (2)**

Yield of 11.8% as white solid; mp (°C): 164-165; IR ν_{max} (KBr) cm^{-1}: 3273, 3193, 3111, 3033, 3009, 1657, 1611, 1537, 1492, 1413, 1343, 1199, 1077, 948, 901, 851, 813, 758, 575, 547, 473; UV λ_{max} ^{MeOH} nm (Log Ɛ): 203.5 (4.7), 246.0 (4.4), 280.0 (4.0, sh); ^{1}H-NMR ($CDCl_3$, 400MHz) δ_H 8.75 (1H, s, NH), 8.29 (1H, dd, *J*= 8.8, 8.4 Hz, H6′), 8.24 (1H, dd, *J*= 9.2, 8.4 Hz, H6″), 8.18

(1H, s, NH), 7.18-7.09 (4H, m, H3′, H3″, H5′, and H5″), 5.99 (1H, s, H_b), 5.86 (1H, s, H_a), 3.50 (2H, s, H3); ^{13}C-NMR ($CDCl_3$, 100MHz) δ_C 168.2 (s, C4), 166.6 (s, C1), 152.6 (d, *J*= 246.0 Hz, C2′ and C2″), 138.6 (s, C2), 129.9 (s, *J*= 9.9 Hz, C4′), 129.2 (s, *J*= 9.9 Hz, C4″), 125.4 (d, *J*= 10.3 Hz, C6″), 124.9 (d, *J*= 9.9 Hz, C6′), 123.6 (t, C5), 122.7 (d, *J*= 15.5 Hz, C1′, and C1″), 116.0 (d, *J*= 22.6 Hz, C3′), 115.8 (d, *J*= 22.5 Hz, C3″), 42.3 (t, C3); ESI-MS (m/z): 407.3 $[M+Na]^+$, 409.2 $[(M+2)+Na]^+$; HRMS calculated for $C_{17}H_{12}Cl_2F_2N_2O_2Na$, $[M+Na]^+$, 407.0136; found 407.0150.

4-((4-chloro-2-fluorophenyl)amino)-2-methylene-4-oxobutanoic acid (2A)

Yield of 4.4% as white solid; mp (°C): 184-185; IR ν_{max} (KBr) cm^{-1}: 3255, 3194, 3113, 3015, 2889, 1668, 1523, 1410, 1359, 1297, 1224, 1165, 1077, 973, 907, 834, 583, 496, 466; UV λ_{max} ^{MeOH} nm (Log Ɛ): 204.0 (4.5), 244.0 (4.2), 280.0 (3.5); ^{1}H-NMR (Acetone-*d6*, 400MHz) δ_H 9.10 (1H, s, NH), 8.24 (1H, dd, *J*= 8.8, 8.4 Hz, H6′), 7.27 (1H, dd, *J*= 11.2, 2.4 Hz, H3′), 7.19 (1H, ddd, *J*= 8.8, 2.8, 1.6 Hz, H5′), 6.32 (1H, d, *J*=0.8 Hz, H_b), 5.86 (1H, s, H_a), 3.52 (2H, s, H3); ^{13}C-NMR (Acetone-*d6*, 100MHz)δ_C 169.5 (s, C1), 168.3 (s, C4), 153.7 (d, *J*= 253.8 Hz, C2′), 136.3 (s, C2), 128.8 (t, C5), 127.1 (d, *J*= 10.6 Hz, C4′), 125.4 (d, *J*= 3.2 Hz, C5′), 124.3 (d, *J*= 11.9 Hz, C6′), 116.6 (d, *J*= 23.1 Hz, C1′, and C3′), 41.0 (t, C3); ESI-MS (m/z): 256.1 $[M-H]^-$, 258.0 $[(M+2)-H]^-$; HRMS calculated for $C_{11}H_8ClFNO_3$, $[M-H]^-$, 256.0171; found 256.0181.

***N*,*N*'-bis(4-bromo-2-fluorophenyl)-2-methylenesuccinamide (3)**

Yield of 8.6% as white solid; mp (°C): 169-170; IR ν_{max} (KBr) cm^{-1}: 3276, 3190, 3093, 3030, 2997, 1677, 1657, 1608, 1534, 1487, 1408, 1340, 1271, 1194, 879, 809, 519, 476; UV λ_{max} ^{MeOH} nm (Log Ɛ): 203.0 (4.7), 248.0 (4.5), 279.5 (4.1, sh); ^{1}H-NMR ($CDCl_3$, 400MHz) δ_H 8.77 (1H, s,

NH), 8.25 (1H, dd, *J*= 8.4, 8.4 Hz, H6″), 8.20 (1H, dd, *J*= 8.8, 8.4 Hz, H6′), 8.18 (1H, s, NH), 7.32-7.23 (4H, m, H3′, H3″, H5′ and H5″), 5.99 (1H, s, H_b), 5.86 (1H, s, H_a), 3.49 (2H, s, H3); ^{13}C-NMR ($CDCl_3$, 100MHz) δ_C 168.2 (s, C4), 166.6 (s, C1), 152.6 (d, *J*= 246.9 Hz, C2″), 152.4 (d, *J*= 247.3 Hz, C2′), 138.5 (s, C2), 128.1 (d, *J*= 3.7 Hz, C6′), 127.8 (d, *J*= 3.6 Hz, C6″), 125.9 (d, *J*= 10.1 Hz, C1′), 125.4 (d, *J*= 10.0 Hz, C1″), 123.7 (t, C5), 123.0 (d, C5′), 122.9 (d, C5″), 118.8 (d, *J*= 22.2 Hz, C3′), 118.6 (d, *J*= 22.1 Hz, C3″), 116.8 (d, *J*= 9.5 Hz, C4′), 116.0 (d, *J*= 9.2 Hz, C4″), 42.3 (t, C3); ESI-MS (m/z): 497.1 $[M+Na]^+$, 499.1 $[(M+2)+Na]^+$; HRMS calculated for $C_{17}H_{12}Br_2F_2N_2O_2Na$, $[M+Na]^+$, 494.9126; found 494.9141.

4-((2-fluoro-4-(trifluoromethyl)phenyl)amino)-2-methylene-4-oxobutanoic acid (3A)

Yield of 8.2% as white solid; mp (°C): 170-171; IR ν_{max} (KBr) cm^{-1}: 3276, 3196, 3110, 3066, 3025, 2916, 2887, 1677, 1631, 1526, 1429, 1334, 1224, 1174, 1131, 979, 914, 570, 456, 432; UV λ_{max}^{MeOH} nm (Log Ɛ): 203.0 (4.5), 246.0 (4.3), 280.0 (3.5); ^{1}H-NMR (Acetone-*d6*, 400MHz) δ_H 9.33 (1H, s, NH), 8.53 (1H, dd, *J*= 8.4, 8.0 Hz, H6′), 7.54-7.51 (4H, m, H3′, and H5′), 6.34 (1H, d, *J*= 0.8 Hz, H_b), 5.88 (1H, s, H_a), 3.58 (2H, s, H3); ^{13}C-NMR (Acetone-*d6*, 100MHz)δ_C 170.0 (s, C1), 168.2 (s, C4), 152.9 (d, *J*= 244.4 Hz, C2′), 136.1 (s, C2), 131.8 (d, *J*= 10.3 Hz, C1′), 129.1 (t, C5), 124.8 (qd, *J*= 269.2, 2.7 Hz, C7′), 126.5-125.5 (m, C4′), 122.7-122.6 (m, C5′), 123.0 (d, C6′), 113.3 (dq, *J*= 22.8, 3.7 Hz, C3′), 41.1 (t, C3); ESI-MS (m/z): 289.7 $[M-H]^-$; HRMS calculated for $C_{12}H_8F_4NO_3$, $[M-H]^-$, 290.0435; found 290.0445.

***N*,*N*'-bis(2-fluoro-4-(trifluoromethyl)phenyl)-2-methylenesuccinamide (4)**

Yield of 8.8% as white solid; mp (°C): 160-161; IR ν_{max} (KBr) cm^{-1}: 3305, 3261, 3116, 3025, 2943, 1669, 1627, 1529, 1504, 1428, 1336, 1175, 1127, 1066, 910, 884, 831, 662, 492, 447; UV

λ_{max} ^{MeOH} nm (Log Ɛ): 203.5 (4.8), 248.5 (4.5); ^{1}H-NMR ($CDCl_3$, 400MHz) δ_H 8.92 (1H, s, NH), 8.54 (1H, dd, *J*= 8.4, 8.0 Hz, H6′), 8.49 (1H, dd, *J*= 8.4, 8.0 Hz, H6″), 8.32 (1H, s, NH), 7.48-7.34 (4H, m, H3′, H3″, H5′, and H5″), 6.04 (1H, s, H_b), 5.92 (1H, s, H_a), 3.55 (2H, s, H3); ^{13}C-NMR ($CDCl_3$, 100MHz) δ_C 168.4 (s, C4), 166.8 (s, C1), 152.0 (d, *J*= 244.3 Hz, C2′), 151.8 (d, *J*= 244.6 Hz, C2″), 138.3 (s, C2), 129.8 (d, *J*= 10.3 Hz, C1′), 129.3 (d, *J*= 9.8 Hz, C1″), 127.3-126.2 (m, C4′, and C4″), 123.4 (qd, *J*= 269.2, 2.7 Hz, C7′, and C7″), 124.2 (t, C5), 122.3-122.0 (m, C5′, and C5″), 121.9 (d, C6′), 121.6 (d, C6″), 112.6 (dq, *J*= 22.4, 3.7 Hz, C3′), 112.4 (dq, *J*= 22.3, 3.7 Hz, C3″), 42.2 (t, C3); ESI-MS (m/z): 451.0 $[M-H]^-$; HRMS calculated for $C_{19}H_{11}F_8N_2O_2$, $[M-H]^-$, 451.0687; found 451.0693.

4-((2,5-difluorophenyl)amino)-2-methylene-4-oxobutanoic acid (4A)

Yield of 12.4% as white solid; mp (°C): 153-154; IR ν_{max} (KBr) cm^{-1}: 3294, 3078, 3015, 2952, 2903, 2871, 1695, 1626, 1551, 1488, 1439, 1282, 1154, 977, 888, 808, 721, 524; UV λ_{max} ^{MeOH} nm (Log Ɛ): 203.0 (4.5), 237.0 (4.2), 275.0 (3.8); ^{1}H-NMR (Acetone-*d6*, 400MHz) δ_H 9.17(1H, s, NH), 8.14 (1H, ddd, *J*= 9.6, 6.4, 3.2 Hz, H6′), 7.18 (1H, ddd, *J*= 9.2, 8.8, 5.2 Hz, H3′), 6.86-6.80 (1H, m, H4′), 6.33 (1H, d, *J*=1.2 Hz, H_b), 5.87 (1H, d, *J*=1.2 Hz, H_a), 3.55 (2H, s, H3); ^{13}C-NMR (Acetone-*d6*, 100MHz)δ_C 169.8 (s, C1), 168.2 (s, C4), 159.5 (d, *J*= 237.1 Hz, C2′), 149.7 (d, *J*= 239.7 Hz, C5′), 136.1 (s, C2), 129.2 (dd, *J*= 12.4, 3.6 Hz, C1′), 129.0 (t, C5), 116.6 (dd, *J*= 22.0, 9.9 Hz, C3′), 110.6 (dd, *J*= 24.6, 7.7 Hz, C4′), 109.6 (dd, *J*= 29.3, 7.8 Hz, C6′), 41.1 (t, C3); ESI-MS (m/z): 240.2 $[M-H]^-$; HRMS calculated for $C_{11}H_8F_2NO_3$, $[M-H]^-$, 240.0467; found 240.0475.

***N*,*N*'-bis(2-fluoro-4-methoxyphenyl)-2-methylenesuccinamide (5)**

Yield of 8.1% as white solid; mp (°C): 144-145; IR ν_{max} (KBr) cm^{-1}: 3275, 3238, 3028, 2946, 2844, 1664, 1627, 1521, 1429, 1273, 1233, 1155, 1113, 1026, 941, 837, 808, 718, 595, 508, 476; UV λ_{max} ^{MeOH} nm (Log Ɛ): 202.0 (4.7), 242.0 (4.3, sh), 278.0 (4.1, sh); ^{1}H-NMR ($CDCl_3$, 400MHz) δ_H 8.60 (1H, s, NH), 8.12 (1H, s, NH), 8.09 (1H, dd, *J*= 9.6, 8.8 Hz, H6″), 8.02 (1H, dd, *J*= 8.8, 8.8 Hz, H6′), 6.72-6.63 (4H, m, H3′, H3″, H5′, and H5″), 5.96 (1H, s, H_b), 5.80 (1H, s, H_a), 3.79 (3H, s, H7″), 3.76 (3H, s, H7′), 3.47 (2H, s, H3); ^{13}C-NMR ($CDCl_3$, 100MHz) δ_C 168.3 (s, C4), 166.6 (s, C1), 157.4 (s, *J*= 10.5 Hz, C5′), 157.0 (s, *J*= 10.1 Hz, C5″), 154.1 (d, *J*= 243.0 Hz, C2′), 154.0 (d, *J*= 243.5 Hz, C2″), 139.0 (s, C2), 123.6 (d, *J*= 10.5 Hz, C6′, and C6″), 122.9 (t, C5), 119.5 (d, *J*= 11.1 Hz, C1′), 118.9 (d, *J*= 10.9 Hz, C1″), 109.7 (d, *J*= 3.0 Hz, C5′), 109.4 (d, *J*= 3.0 Hz, C5″), 102.0 (d, *J*= 22.8 Hz, C3′), 101.9 (d, *J*= 22.7 Hz, C3″), 55.9 (q, C7′, and C7″), 42.1 (t, C3); ESI-MS (m/z): 375.3 $[M-H]^-$; HRMS calculated for $C_{19}H_{17}F_2N_2O_4$, $[M-H]^-$, 375.1151; found 375.1159.

4-((2-fluoro-5-(trifluoromethyl)phenyl)amino)-2-methylene-4-oxobutanoic (5A)

Yield of 9.0% as brown solid; mp (°C): 144-145; IR ν_{max} (KBr) cm^{-1}: 3264, 3151, 3106, 3064, 3018, 2908, 2853, 1687, 1627, 1542, 1489, 1437, 1335, 1263, 1228, 1169, 1124, 1064, 977, 918, 825, 689, 512, 487; UV λ_{max} ^{MeOH} nm (Log Ɛ): 203.0 (4.4), 241.0 (4.0); ^{1}H-NMR (Acetone-*d6*, 400MHz) δ_H 9.34 (1H, s, NH), 8.71 (1H, dd, *J*= 7.2, 2.0 Hz, H6′), 7.48-7.44 (1H, m, H4′), 7.40 (1H, dd, *J*= 10.4, 8.8 Hz, H3′), 6.34 (1H, d, *J*= 1.2 Hz, H_b), 5.88 (1H, d, *J*= 1.2 Hz, H_a), 3.57 (2H, s, H3); ^{13}C-NMR (Acetone-*d6*, 100MHz)δ_C 170.1 (s, C1), 168.2 (s, C4), 155.4 (d, *J*= 248.6 Hz, C2′), 136.1 (s, C2), 129.0 (t, C5), 128.9 (d, *J*= 15.5 Hz, C1′), 127.6-126.8 (m, C5′), 125.1 (q, *J*= 269.6 Hz, C7′), 122.2 (d, C4′), 119.9 (d, C6′), 116.9 (d, *J*= 21.0 Hz, C3′), 41.0 (t, C3); ESI-MS (m/z): 289.9 $[M-H]^-$; HRMS calculated for $C_{12}H_8F_4NO_3$, $[M-H]^-$, 290.0435; found 290.0442.

_N_,_N_'-bis(2,5-difluorophenyl)-2-methylenesuccinamide (6)

Yield of 21.2% as white solid; mp (°C): 140-141; IR ν_{max} (KBr) cm^{-1}: 3393, 3301, 3285, 3255, 3222, 3141, 3089, 3024, 2962, 1682, 1628, 1548, 1487, 1438, 1197, 967, 866, 805, 526, 462. UV λ_{max} ^{MeOH} nm (Log Ɛ): 202.5 (4.5), 239.0 (4.2), 277.5 (4.0); ^{1}H-NMR ($CDCl_3$, 400MHz) δ_H 8.82 (1H, s, NH), 8.24 (1H, s, NH), 8.19 (1H, ddd, *J*= 10.4, 6.4, 3.2 Hz, H6′), 8.13 (1H, ddd, *J*= 10.4, 6.4, 3.2 Hz, H6″), 7.10-6.99 (2H, m, H3′ and H3″), 6.81-6.69 (2H, m, H4′ and H4″), 6.00 (1H, s, H_b), 5.88 (1H, s, H_a), 3.51 (2H, s, H3); ^{13}C-NMR ($CDCl_3$, 100MHz) δ_C 168.2 (s, C4), 166.6 (s, C1), 158.7 (d, *J*= 243.0 Hz, C5′, and C5″) 148.8 (d, *J*= 235.3 Hz, C2′) 148.6 (d, *J*= 235.3 Hz, C2″), 138.5 (s, C2), 127.4 (dd, *J*= 12.2, 12.0 Hz, C1′), 126.9 (dd, *J*= 12.1, 11.7 Hz, C1″), 123.7 (t, C5), 115.7-115.2 (m, C6′, and C6″), 111.0 (dd, *J*= 24.4, 7.7 Hz, C3′), 110.3 (dd, *J*= 24.4, 7.7 Hz, C3″), 109.1 (dd, *J*= 30.1, 16.5 Hz, C4′, and C4″), 42.2 (t, C3); ESI-MS (m/z): 353.1 $[M+H]^+$, 375.2 $[M+Na]^+$; HRMS calculated for $C_{17}H_{13}F_4N_2O_2$, $[M+H]^+$, 353.0908; found 353.0912.

4-((5-chloro-2-fluorophenyl)amino)-2-methylene-4-oxobutanoic acid (6A)

Yield of 9.9% as white solid; mp (°C): 171-172; IR ν_{max} (KBr) cm^{-1}: 3266, 3123, 3092, 3048, 3018, 2919, 2886, 1700, 1667, 1609, 1536, 1488, 1414, 1238, 1196, 963, 907, 803, 704, 523, 503; UV λ_{max} ^{MeOH} nm (Log Ɛ): 206.0 (4.6), 241.0 (4.2), 280.0 (3.6); ^{1}H-NMR (Acetone-*d6*, 400MHz) δ_H 9.17(1H, s, NH), 8.38 (1H, ddd, *J*= 6.8, 6.4, 2.4 Hz, H6′), 7.20 (1H, dd, *J*= 10.8, 8.8 Hz, H3′), 7.12-7.08 (1H, m, H4′), 6.33 (1H, d, *J*=1.2 Hz, H_b), 5.87 (1H, d, *J*=1.2 Hz, H_a), 3.55 (2H, s, H3); ^{13}C-NMR (Acetone-*d6*, 100MHz)δ_C 169.8 (s, C1), 168.1 (s, C4), 152.2 (d, *J*= 242.2 Hz, C2′), 136.2 (s, C2), 129.8 (d, *J*= 3.3 Hz, C5′), 129.2 (d, *J*= 12.2 Hz, C1′), 129.0 (t, C5), 124.5 (d, *J*=

7.7 Hz, C4′), 122.5 (d, C6′), 117.3 (d, *J*= 21.1 Hz, C3′), 41.0 (t, C3); ESI-MS (m/z): 256.3 $[M-H]^-$, 258.2 $[(M+2)-H]^-$; HRMS calculated for $C_{11}H_8ClFNO_3$, $[M-H]^-$, 256.0171; found 256.0181.

_N_,_N_'-bis(5-chloro-2-fluorophenyl)-2-methylenesuccinamide (7)

Yield of 11.7% as white solid; mp (°C): 140-141; IR ν_{max} (KBr) cm^{-1}: 3333, 3265, 3247, 3114, 3091, 3019, 1678, 1631, 1611, 1538, 1519, 1489, 1416, 1393, 1324, 1257, 1222, 1186, 1148, 1111, 937, 875, 812, 708, 647, 462; UV λ_{max} ^{MeOH} nm (Log Ɛ): 205.0 (4.7), 242.0 (4.3), 279.0 (3.9); ^{1}H-NMR ($CDCl_3$, 400MHz) δ_H 8.73 (1H, s, NH), 8.40 (1H, dd, *J*= 7.6, 5.6 Hz, H6′), 8.35 (1H, dd, *J*= 7.6, 5.6 Hz, H6″), 8.21 (1H, s, NH), 7.07-6.99 (4H, m, H3′, H3″, H4′, and H4″), 5.99 (1H, s, H_b), 5.87 (1H, s, H_a), 3.50 (2H, s, H3); ^{13}C-NMR ($CDCl_3$, 100MHz) δ_C 168.2 (s, C4), 166.6 (s, C1), 151.3 (d, *J*= 242.3 Hz, C2′), 151.2 (d, *J*= 242.5 Hz, C2″), 138.5 (s, C2), 130.1 (d, *J*= 3.3 Hz, C5′), 129.8 (s, *J*= 3.2 Hz, C5″), 127.4 (d, *J*= 11.6 Hz, C4″), 127.0 (d, *J*= 11.4 Hz, C4′), 124.8 (d, *J*= 7.7 Hz, C6′), 124.2 (d, *J*= 7.4 Hz, C6″), 123.7 (t, C5), 121.8 (d, *J*= 12.3 Hz, C1′, and C1″), 115.9 (d, *J*= 20.8 Hz, C3′), 115.8 (d, *J*= 20.8 Hz, C3″), 42.1 (t, C3); ESI-MS (m/z): 407.3 $[M+Na]^+$, 409.2 $[(M+2)+Na]^+$; HRMS calculated for $C_{17}H_{12}Cl_2F_2N_2O_2Na$, $[M+Na]^+$, 407.0136; found 407.0151.

4-((4-fluoro-2-(trifluoromethyl)phenyl)amino)-2-methylene-4-oxobutanoic acid (7A)

Yield of 6.2% as white solid; mp (°C): 146-148; IR ν_{max} (KBr) cm^{-1}: 3274, 3150, 3087, 3015, 2979, 2925, 2885, 1700, 1665, 1533, 1433, 1323, 1279, 1246, 1171, 1131, 1048, 964, 915, 876, 836, 668, 576, 497, 422; UV λ_{max} ^{MeOH} nm (Log Ɛ): 203.0 (4.4), 231.0 (3.9), 272.0 (3.4); ^{1}H-NMR (Acetone-*d6*, 400MHz) δ_H 8.72 (1H, s, NH), 7.91-7.86 (1H, m, H6′), 7.50-7.42 (1H, m, H3′, H5′), 6.34 (1H, s, H_b), 5.89 (1H, s, H_a), 3.48 (2H, s, H3); ^{13}C-NMR (Acetone-*d6*,

100MHz)δ_C 169.9 (s, C1), 168.3 (s, C4), 160.3 (d, *J*= 243.7 Hz, C4′), 136.3 (s, C2), 133.1 (brs, C1′), 131.2 (brd, C6′), 129.0 (t, C5), 128.2-120.0 (m, C2′, and C7′), 120.5 (d, *J*= 22.0 Hz, C5′), 114.2 (dq, *J*= 26.3, 5.5 Hz, C3′), 40.8 (t, C3); ESI-MS (m/z): 290.2 $[M-H]^-$; HRMS calculated for $C_{12}H_8F_4NO_3$, $[M-H]^-$, 290.0435; found 290.0439.

_N_,_N_'-bis(2-fluoro-5-(trifluoromethyl)phenyl)-2-methylenesuccinamide (8)

Yield of 12.3% as white solid; mp (°C): 90-92; IR ν_{max} (KBr) cm^{-1}: 3268, 3163, 3094, 3027, 1670, 1622, 1550, 1491, 1438, 1338, 1267, 1174, 1128, 1070, 942, 898, 823, 606, 556, 524, 457; UV λ_{max}^{MeOH} nm (Log Ɛ): 203.0 (4.8), 243.5 (4.4); ^{1}H-NMR ($CDCl_3$, 400MHz) δ_H 8.82 (1H, s, NH), 8.71 (1H, dd, *J*= 7.2, 2.0 Hz, H6′), 8.65 (1H, d, *J*= 7.2 Hz, H6″), 8.30 (1H, s, NH), 7.41-7.38 (1H, m, H4′), 7.34-7.31 (1H, m, H4″), 7.24 (1H, dd, *J*= 9.2, 9.2 Hz, H3′), 7.18 (1H, dd, *J*= 10.0, 9.2 Hz, H3″), 6.03 (1H, s, H_b), 5.90 (1H, s, H_a), 3.55 (2H, s, H3); ^{13}C-NMR ($CDCl_3$, 100MHz) δ_C 168.5 (s, C4), 166.8 (s, C1), 154.4 (d, *J*= 247.5 Hz, C2′), 154.2 (d, *J*= 248.0 Hz, C2″), 138.3 (s, C2), 128.0-127.1 (m, C5′, and C5″), 127.1 (d, *J*= 11.2 Hz, C1″), 126.7 (d, *J*= 10.8 Hz, C1′), 123.7 (qd, *J*= 269.9, 6.8 Hz, C7′, and C7″), 124.1 (t, C5), 122.4-121.7 (m, C4′, and C4″), 119.7-119.3 (m, C6′, and C6″), 115.6 (d, *J*= 20.6 Hz, C3′), 115.5 (d, *J*= 20.6 Hz, C3″), 42.0 (t, C3); ESI-MS (m/z): 451.1 $[M-H]^-$; HRMS calculated for $C_{19}H_{11}F_8N_2O_2$, $[M-H]^-$, 451.0687; found 451.0693.

4-((5-fluoro-2-(trifluoromethyl)phenyl)amino)-2-methylene-4-oxobutanoic acid (8A)

Yield of 9.2% as white solid; mp (°C): 147-148; IR ν_{max} (KBr) cm^{-1}: 3283, 3099, 3048, 3016, 2926, 2865, 1703, 1676, 1605, 1537, 1496, 1438, 1395, 1316, 1235, 1159, 1117, 1048, 968, 944, 872, 827, 657, 585, 492, 455, 414; UV λ_{max}^{MeOH} nm (Log Ɛ): 204.0 (4.5), 239.0 (4.1); ^{1}H-NMR

(Acetone-*d6*, 400MHz) δ_H 8.74 (1H, s, NH), 7.98-7.93 (1H, m, H6′), 7.76 (1H, dd, *J*= 8.8, 8.8 Hz, H3′), 7.14-7.09 (1H, m, H4′), 6.37 (1H, d, *J*= 0.8 Hz, H_b), 5.94 (1H, s, H_a), 3.52 (2H, s, H3); ^{13}C-NMR (Acetone-*d6*, 100MHz)δ_C 169.7 (s, C1), 168.2 (s, C4), 165.7 (d, *J*= 247.7 Hz, C5′), 139.3-139.1 (m, C1′), 135.9 (s, C2), 129.6-129.4 (m, C5, C6′), 124.8 (q, *J*= 270.3 Hz, C7′), 118.1-117.8 (m, C2′), 113.5-113.1 (m, C3′), 112.6-112.3 (m, C4′), 41.4 (t, C3); ESI-MS (m/z): 290.2 $[M-H]^-$; HRMS calculated for $C_{12}H_8F_4NO_3$, $[M-H]^-$, 290.0435; found 290.0440.

_N_,_N_'-bis(2-fluoro-5-methoxyphenyl)-2-methylenesuccinamide (9)

Yield of 7.2% as white solid; mp (°C): 121-122; IR ν_{max} (KBr) cm^{-1}: 3301, 3154, 3066, 3006, 2946, 2835, 1672, 1618, 1541, 1482, 1428, 1353, 1316, 1252, 1211, 1038, 957, 867, 807, 716, 547, 468; UV λ_{max} ^{MeOH} nm (Log Ɛ): 204.0 (4.7), 239.0 (4.3), 289.0 (4.1); ^{1}H-NMR ($CDCl_3$, 400MHz) δ_H 8.72 (1H, s, NH), 8.23 (1H, s, NH), 8.00 (1H, dd, *J*= 6.4, 3.2 Hz, H6′), 7.95 (1H, dd, *J*= 6.4, 3.2 Hz, H6″), 7.01 (1H, dd, *J*= 9.2, 8.8 Hz, H3′), 6.96 (1H, dd, *J*= 9.2, 8.8 Hz, H3″), 6.60 (1H, ddd, *J*= 8.8, 7.2, 3.6 Hz, H4′), 6.54 (1H, ddd, *J*= 8.8, 7.2, 3.6 Hz, H4″), 5.98 (1H, s, H_b), 5.84 (1H, s, H_a), 3.80 (3H, s, H7′), 3.77 (3H, s, H7″), 3.51 (2H, s, H3); ^{13}C-NMR ($CDCl_3$, 100MHz) δ_C 168.3 (s, C4), 166.5 (s, C1), 156.1 (s, C5′), 156.0 (s, C5″), 147.3 (d, *J*= 234.8 Hz, C2′), 147.2 (d, *J*= 235.0 Hz, C2″), 138.9 (s, C2), 127.0 (d, *J*= 11.6 Hz, C4″), 126.5 (d, *J*= 11.5 Hz, C4′), 123.2 (t, C5), 115.2 (d, *J*= 20.7 Hz, C3′), 115.1 (d, *J*= 20.6 Hz, C3″), 110.4 (d, *J*= 7.2 Hz, C6′), 109.8 (d, *J*= 7.2 Hz, C6″), 106.9 (d, *J*= 11.2 Hz, C1′, and C1″), 55.9 (q, C7′, and C7″), 42.3 (t, C3); ESI-MS (m/z): 375.1 $[M-H]^-$; HRMS calculated for $C_{19}H_{17}F_2N_2O_4$, $[M-H]^-$, 375.1151; found 375.1158.

2-methylene-4-oxo-4-((2-(trifluoromethyl)phenyl)amino)butanoic acid (9A)

Yield of 11.2% as white solid; mp (°C): 153-154; IR ν_{max} (KBr) cm^{-1}: 3298, 3214, 3130, 3059, 3013, 2910, 2864, 1703, 1676, 1637, 1593, 1537, 1451, 1393, 1320, 1290, 1235, 1163, 1122, 1051, 948, 902, 764, 653, 512, 454; UV λ_{max} ^{MeOH} nm (Log Ɛ): 203.0 (4.4), 233.0 (3.9), 269.0 (3.3); ^{1}H-NMR (Acetone-*d6*, 400MHz) δ_H 8.68 (1H, s, NH), 7.98-7.94 (1H, m, H3′), 7.69 (1H, d, *J*= 7.6 Hz, H6′), 7.64 (1H, dd, *J*= 8.0, 7.6 Hz, H5′), 7.36 (1H, dd, *J*= 7.6, 7.6 Hz, H4′), 6.35 (1H, d, *J*= 1.6 Hz, H_b), 5.91 (1H, d, *J*= 1.2 Hz, H_a), 3.50 (2H, s, H3); ^{13}C-NMR (Acetone-*d6*, 100MHz)δ_C 169.6 (s, C1), 168.3 (s, C4), 136.8 (brs, C1′), 136.3 (s, C2), 133.7 (d, C5′), 129.0 (t, C5), 127.8 (brd, C3′), 126.9 (q, *J*= 5.3 Hz, C6′), 126.2 (d, C4′), 125.0 (q, *J*= 270.9 Hz, C7′), 123.1-122.5 (m, C2′), 41.0 (t, C3); ESI-MS (m/z): 271.8 $[M-H]^-$.

_N_,_N_'-bis(2-bromo-4-fluorophenyl)-2-methylenesuccinamide (10)

Yield of 6.6% as white solid; mp (°C): 165-166; IR ν_{max} (KBr) cm^{-1}: 3263, 3193, 3110, 3033, 3006, 1655, 1629, 1599, 1527, 1484, 1390, 1315, 1261, 1189, 1141, 817, 657, 513, 482, 443; UV λ_{max} ^{MeOH} nm (Log Ɛ): 205.0 (4.7), 243.0 (4.1, sh), 277.0 (3.7, sh); ^{1}H-NMR ($CDCl_3$, 400MHz) δ_H 8.51 (1H, s, NH), 8.34 (1H, dd, *J*= 9.2, 5.6 Hz, H6′), 8.27 (1H, s, NH), 8.22 (1H, dd, *J*= 9.2, 5.6 Hz, H6″), 7.33 (1H, dd, *J*= 7.6, 2.8 Hz, H3′), 7.28 (1H, dd, *J*= 8.0, 2.8 Hz, H3″), 7.08(1H, ddd, *J*= 8.0, 8.0, 2.8 Hz, H5′), 7.03 (1H, ddd, *J*= 8.4, 8.0, 2.8 Hz, H5″), 6.05 (1H, s, H_b), 5.90 (1H, s, H_a), 3.55 (2H, s, H3); ^{13}C-NMR ($CDCl_3$, 100MHz) δ_C 168.1 (s, C4), 166.1 (s, C1), 159.0 (d, *J*= 247.6 Hz, C4′ and C4″), 139.8 (s, C2), 132.5 (s, *J*= 3.2 Hz, C1′), 131.9 (s, *J*= 3.2 Hz, C1″), 123.8 (d, *J*= 7.7 Hz, C6″), 123.3 (d, *J*= 8.2 Hz, C6′), 123.1 (t, C5), 119.7 (d, *J*= 25.7 Hz, C3′), 119.6 (d, *J*= 25.3 Hz, C3″), 115.5 (d, *J*= 21.8 Hz, C5′), 115.2 (d, *J*= 21.4 Hz, C5″), 114.4 (s, C2′), 114.3 (s, C2″), 42.0 (t, C3); ESI-MS (m/z): 472.7 $[M-H]^-$, 474.7 $[(M+2)-H]^-$; HRMS calculated for $C_{17}H_{11}Br_2F_2N_2O_2$, $[M-H]^-$, 470.9150; found 470.9167.

2-methylene-4-oxo-4-((3-(trifluoromethyl)phenyl)amino)butanoic acid (10A)

Yield of 12.2% as white solid; mp (°C): 132-133; IR ν_{max} (KBr) cm^{-1}: 3286, 3195, 3143, 3112, 3078, 3006, 2907, 1690, 1656, 1599, 1532, 1445, 1334, 1246, 1170, 1136, 1066, 978, 902, 701, 535, 493 UV λ_{max}^{MeOH} nm (Log Ɛ): 203.5 (4.6), 244.0 (4.3); ^{1}H-NMR (Acetone-*d6*, 400MHz) δ_H 9.54 (1H, s, NH), 8.16 (1H, s, H2′), 7.81 (1H, d, *J*= 8.0 Hz, H6′), 7.52 (1H, t, *J*= 8.0 Hz, H5′), 7.37 (1H, d, *J*= 7.6 Hz, H4′), 6.32 (1H, d, *J*= 1.2 Hz, H_b), 5.84 (1H, d, *J*= 1.2 Hz, H_a), 3.46 (2H, s, H3); ^{13}C-NMR (Acetone-*d6*, 100MHz)δ_C 169.6 (s, C1), 167.9 (s, C4), 141.1 (s, C1′), 136.1 (s, C2), 131.3 (q, *J*= 31.7 Hz, C3′), 130.6 (d, C5′), 129.3 (t, C5), 125.2 (q, *J*= 269.9 Hz, C7′), 123.3 (d, C6′), 120.5-120.4 (m, C4′), 116.4-116.3 (m, C2′), 40.9 (t, C3); ESI-MS (m/z): 272.1 $[M-H]^-$; HRMS calculated for $C_{12}H_9F_3NO_3$, $[M-H]^-$, 272.0529; found 272.0535.

***N*,*N*'-bis(4-fluoro-2-(trifluoromethyl)phenyl)-2-methylenesuccinamide (11)**

Yield of 5.6% as white solid; mp (°C): 130-131; IR ν_{max} (KBr) cm^{-1}: 3278, 3084, 3017, 2927, 2846, 1671, 1628, 1531, 1505, 1433, 1319, 1277, 1251, 1204, 1167, 1129, 1049, 912, 882, 831, 741, 672, 637, 525; UV λ_{max}^{MeOH} nm (Log Ɛ): 204.0 (4.2), 232.0 (4.1), 272.0 (3.7); ^{1}H-NMR ($CDCl_3$, 400MHz) δ_H 8.50 (1H, s, NH), 8.15 (1H, dd, *J*= 9.2, 8.8 Hz, H6′), 8.10 (1H, s, NH), 8.00 (1H, dd, *J*= 8.8, 8.8 Hz, H6″), 7.38-7.22 (4H, m, H3′, H3″, H5′, and H5″), 5.98 (1H, s, H_b), 5.89 (1H, s, H_a), 3.51 (2H, s, H3); ^{13}C-NMR ($CDCl_3$, 100MHz) δ_C 168.6 (s, C4), 166.6 (s, C1), 159.4 (d, *J*= 246.3 Hz, C4′), 159.2 (d, *J*= 246.0 Hz, C4″), 138.5 (s, C2), 131.3 (s, C1′), 130.9 (s, C1″), 128.2 (d, *J*= 7.6 Hz, C6″), 127.5 (d, *J*= 7.8 Hz, C6′), 123.4 (t, C5), 124.6-121.7 (m, C2′, C2″, C7′, and C7″), 119.9 (d, *J*= 21.8 Hz, C5′), 119.6 (d, *J*= 21.7 Hz, C5″), 114.0-113.5 (m, C3′

and C3″), 41.8 (t, C3); ESI-MS (m/z): 451.1 $[M-H]^-$; HRMS calculated for $C_{19}H_{11}F_8N_2O_2$, $[M-H]^-$, 451.0687; found 451.0692.

2-methylene-*N*,*N*'-bis(2-(trifluoromethyl)phenyl)succinamide (12)

Yield of 6.6% as white solid; mp (°C): 131-132; IR ν_{max} (KBr) cm^{-1}: 3278, 3120, 3047, 3008, 2926, 2846, 1670, 1631, 1588, 1525, 1456, 1322, 1280, 1161, 1113, 1060, 1038, 943, 761, 654, 497, 430; UV λ_{max} ^{MeOH} nm (Log Ɛ): 204.0 (4.6), 233.0 (4.2), 272.0 (3.7, sh); ^{1}H-NMR ($CDCl_3$, 400MHz) δ_H 8.55 (1H, s, NH), 8.26 (1H, d, *J*= 8.4 Hz, H6′), 8.20 (1H, s, NH), 8.09 (1H, d, *J*= 8.0 Hz, H6″), 7.65-7.52 (4H, m, H3′, H3″, H5′, and H5″), 7.29-7.21 (2H, m, H4′, and H4″), 5.98 (1H, s, H_b), 5.89 (1H, s, H_a), 3.53 (2H, s, H3); ^{13}C-NMR ($CDCl_3$, 100MHz) δ_C 168.5 (s, C4), 166.4 (s, C1), 138.9 (s, C2), 135.3 (s, C1′), 135.0 (s, C1″), 133.2 (d, C5′), 132.8 (d, C5″), 126.4-126.1 (m, C3′ and C3″), 125.5 (d, C4″), 125.1 (d, C6″), 124.9 (d, C4′), 124.6 (d, C6′), 124.3 (q, *J*= 271.4 Hz, C7′), 124.0 (q, *J*= 271.4 Hz, C7″), 123.0 (t, C5), 121.2-120.3 (q, C2′, and C2″), 119.9 (d, *J*= 21.8 Hz, C5′), 119.6 (d, *J*= 21.7 Hz, C5″), 41.8 (t, C3); ESI-MS (m/z): 415.2 $[M-H]^-$; HRMS calculated for $C_{19}H_{13}F_6N_2O_2$, $[M-H]^-$, 415.0876; found 415.0891.

***N*,*N*'-bis(2,4-dibromophenyl)-2-methylenesuccinamide (13)**

Yield of 7.8% as white solid; mp (°C): 195-196; IR ν_{max} (KBr) cm^{-1}: 3407, 3299, 3256, 3076, 3025, 2947, 1660, 1576, 1524, 1464, 1375, 1312, 1282, 1194, 861, 819, 543, 483, 445; UV λ_{max} ^{MeOH} nm (Log Ɛ): 206.5 (4.8), 251.0 (4.3); ^{1}H-NMR ($CDCl_3$, 400MHz) δ_H 8.56 (1H, s, NH), 8.34 (1H, s, NH), 8.31 (1H, d, *J*= 8.8 Hz, H6′), 8.21 (1H, d, *J*= 8.8 Hz, H6″), 7.71 (1H, d, *J*= 2.0 Hz, H3′), 7.67 (1H, d, *J*= 2.0 Hz, H3″), 7.46 (1H, dd, *J*= 8.8, 2.0 Hz, H5′), 7.40 (1H, dd, *J*= 8.8, 2.0 Hz, H5″), 6.05 (1H, s, H_b), 5.91 (1H, s, H_a), 3.54 (2H, s, H3); ^{13}C-NMR ($CDCl_3$, 100MHz) δ_C

168.1 (s, C4), 165.9 (s, C1), 138.9 (s, C2), 135.3 (s, C1′), 134.7 (d, C3′, and C3″), 134.6 (s, C1″), 131.7 (d, C5′), 131.4 (d, C5″), 123.3 (t, C5), 122.9 (d, C6′ and C6″), 117.5 (s, C2′), 117.5 (s, C2″), 114.4 (s, C4′), 114.3 (s, C4″) 42.1 (t, C3); ITMS +c ESI-MS (m/z): 618.9 $[M+Na]^+$, 620.8 $[(M+2)+Na]^+$; HRMS calculated for $C_{17}H_{12}Br_4N_2O_2Na$, $[M+Na]^+$, 618.7484; found 618.7498.

***N*,*N*'-bis(2,4-difluorobenzyl)-2-methylenesuccinamide (14)**

Yield of 11.4% as white solid; mp (°C): 143-144; IR ν_{max} (KBr) cm^{-1}: 3303, 3174, 3063, 2946, 2858, 1654, 1615, 1540, 1510, 1429, 1273, 1245, 1141, 1096, 1017, 962, 850, 731, 511, 469; UV λ_{max} ^{MeOH} nm (Log Ɛ): 203.0 (4.4), 259.0 (3.3, sh), 268.0 (3.2, sh); ^{1}H-NMR ($CDCl_3$, 400MHz) δ_H 7.33-7.22 (2H, m, H6′ and H6″), 7.00 (2H, s, NH), 6.84-6.75 (4H, m, H3′, H3″, H5′ and H5″), 5.78 (1H, s, H_b), 5.55 (1H, s, H_a), 4.47 (2H, d, *J*= 6.0 Hz, H7′), 4.38 (2H, d, *J*= 6.0 Hz, H7″), 3.23 (2H, s, H3); ^{13}C-NMR ($CDCl_3$, 100MHz)δ_C 170.4 (s, C4), 168.5 (s, C1), 162.6 (dd, *J*= 245.9, 12.6 Hz, C2′, and C2″), 161.1 (dd, *J*= 247.2, 12.3 Hz, C4′, and C4″), 138.7 (s, C2), 131.2 (dd, *J*= 9.4, 9.7 Hz, C6′), 130.9 (dd, *J*= 9.7, 9.7 Hz, C6″), 122.5 (t, C5), 121.3 (dd, *J*= 14.7, 3.6 Hz, C1′), 121.0 (dd, *J*= 15.0, 3.6 Hz, C1″), 111.6 (dd, *J*= 12.1, 3.7 Hz, C5′), 111.4 (dd, *J*= 12.1, 3.7 Hz, C5″), 104.2 (dd, *J*= 25.2, 25.2 Hz, C3′), 103.9 (dd, *J*= 25.2, 25.3 Hz, C3″), 41.2 (t, C3), 37.5 (t, *J*= 3.5 Hz, C7′), 37.2 (t, *J*= 3.8 Hz, C7″); ESI-MS (m/z): 381.2 $[M+H]^+$, 403.2 $[M+Na]^+$; HRMS calculated for $C_{19}H_{16}F_4N_2O_2Na$, $[M+Na]^+$, 403.1040; found 403.1046.

***N*,*N*'-bis(2,5-difluorobenzyl)-2-methylenesuccinamide (15)**

Yield of 14.2% as white solid; mp (°C): 153-154; IR ν_{max} (KBr) cm^{-1}: 3336, 3060, 2925, 1658, 1618, 1538, 1494, 1433, 1263, 1186, 1022, 947, 881, 807, 714, 543, 493, 441; UV λ_{max} ^{MeOH} nm (Log Ɛ): 203.0 (4.4), 267.0 (3.7, sh), 273.0 (3.6, sh); ^{1}H-NMR ($CDCl_3$, 400MHz) δ_H 7.06-6.88

(7H, m, NH, H3′, H3″, H4′, H4″, H6′ and H6″), 6.85 (1H, s, NH), 5.81 (1H, s, H_b), 5.62 (1H, s, H_b), 4.52 (2H, d, *J*= 6.0 Hz, H7′), 4.43 (2H, d, *J*= 6.0 Hz, H7″), 3.28 (2H, s, H3); ^{13}C-NMR ($CDCl_3$, 100MHz)δ_C 170.4 (s, C4), 168.6 (s, C1), 158.8 (d, *J*= 239.3 Hz, C5′, C5″, C2′, and C2″), 138.6 (s, C2), 127.2-126.9 (m, C1′ and C1″), 122.6 (t, C5), 116.8-115.3 (m, C3′, C3″, C4′, C4″, C6′ and C6″), 41.3 (t, C3), 37.8 (t, C7′), 37.5 (t, C7″); ESI-MS (m/z): 381.5 $[M+H]^+$, 403.3 $[M+Na]^+$; HRMS calculated for $C_{19}H_{16}F_4N_2O_2Na$, $[M+Na]^+$, 403.1040; found 403.1053.

Biology: cells, viruses, and chemicals

The information regarding all the clinical enterovirus strains and influenza viruses listed in **Table 1** is the same as that reported previously.[32] MDCK cells used for IAV infection was cultured in E10 (DMEM containing 10% FBS, 100 U/ml penicillin (Gibco, USA), 100 μg/ml streptomycin (Gibco, USA), 2 mM L-glutamine (L-glutamine) (Gibco, Brazil), 0.1 mM non-essential amino acid mixture (NEAA, Gibco, USA)). The E0 medium is the same as E10, except for FBS. RD cells were used to infect enterovirus and rhinovirus, and cultured in DMEM containing 10% FBS with 100 U/ml penicillin (Gibco, USA), and 100 μg/ml streptomycin (Gibco, USA). All cells were maintained in a 37 °C incubator with 5% carbon dioxide.

Half-maximal effectiveness assay (EC_{50} assay)

The 96-well tissue culture plates were seeded with MDCK cells (2×10^4 per well) or RD cells (2×10^4 cells /well) in E10 medium and incubated under 5% CO_2 for 16–24 h at 37°C. Then, the culture medium was withdrawn, and the wells were washed once with Dulbecco's phosphate-buffered saline (DPBS). Then, the cells were infected with influenza virus (A/WSN/33) or

enteroviruses at a nine-fold median tissue culture infective dose, with or without the addition of distinct concentrations of the synthesized compounds. The treated cells were further incubated for 72 h at 37°C in an incubator containing 5% CO_2. After 72 h, the medium was removed, and the cells were fixed with 4% paraformaldehyde for 1 h at room temperature. Then, 0.1% crystal violet was used to stain the cells for 20 min at room temperature. The cell density was measured by using a VICTOR3™ multilabel plate reader (PerkinElmer). The EC_{50} value was calculated by using the Reed–Muench method as the concentration of the compound that could inhibit virus-CPE by 50%.[33]

Cytotoxicity Test (CC_{50} assay)

MDCK cells, or RD cells were cultured in a 96-well plate (2×10^4 cells per well) in E10 medium and incubated at 37°C under 5% CO_2 overnight. Then, the wells were washed once with DPBS. Next, various concentrations of the synthetic compounds were added and further incubated under 5% CO_2, at 37°C for 72 h. The cell wells were washed again with DPBS, and 50 μL of 3-(4,5-dimethylthiazol-2-yl)-2,5-diphenyltetrazolium bromide (MTT) was loaded into each well and incubated for 3 h at 37°C with 5% CO_2. The medium was removed, 200 μL of dimethyl sulfoxide was added to each well to dissolve the formazan crystals, and the cell density of each well was measured at 570 nm on a VICTOR3. Then, the median cytotoxic concentration (CC_{50}) was calculated by the Reed–Muench method based on the concentration of the compound responsible for 50% cell death.[33]

Cytopathic effect (CPE) detection

MDCK cells (2×10^5 cell/well) were uniformly seeded into a six-well culture dish, placed in a 37°C incubator with 5% CO_2 for 16–24 h, infected with 0.5 multiplicity of infection (MOI) of influenza strain A/WSN/33 for 1 h, and then rinsed twice with DPBS. E0 medium containing 10 μM of compound **1** was added and incubated at 37°C for different time points. CPE production was observed by using a microscope (Zeiss Axiovert 200M; 20x objective lens) at 12 and 36 h pi.[34]

Hemagglutination inhibition assay (HAI)

In this experiment, guinea pig RBCs were used as a material for detecting the activity of influenza virus HA. First, we determined the hemagglutination unit of blood agglutination by diluting the virus stock solution (50 μL/well) in two-fold sequence, then we added 0.5% RBCs (50 μL/well) to the round-bottom 96-well plates. After 1 h, the amount of virus capable of agglutinating the RBCs at the maximum dilution was defined as 1HAv, and the amount of 4HAv virus was taken for HAI assay. In the HAI assay, the drug was diluted in two-fold sequence (25 μL/well), 4HAv virus was added (25 μL/well), and the wells were kept at room temperature for 30 min. Then, 0.5% RBCs were added (50 μL/well) to the well, and the phenomenon of RBC agglutination was observed after 1 h.[34]

Time-of-addition assay

MDCK cells (5×10^5 cells/well) were uniformly seeded into a six-well culture dish and placed in a 37°C incubator with 5% CO_2. After the cells grew into a single layer, the culture solution was removed. The cells were washed once with DPBS, compound **1** (10 μM) was added at different time points at pi = −3 to 9, −1 to 9, 0 to 9, 3 to 9, 6 to 9 h, and the virus adsorption was between

−1 and 0 h pi with MOI = 0.1. One hour after influenza A/WSN/33 virus infection, the virus solution was aspirated and washed once with PBS, and the supernatant was collected after 9 h pi to test for plaque changes.[34]

RNA purification and quantitative reverse transcription-PCR (RT-qPCR)

MDCK cells (5×10^5 cell /well) were seeded into a six-well plate and placed in a 37°C incubator with 5% CO_2 for 16–24 h. After the cells grew into a single layer every other day, the culture was removed. The solution was washed once with HBSS and infected with the virus A/WSN/33 of MOI = 0.01 for 1 h in E0. Then, using the reagent TRIzol (Invitrogen, Carlsbad, CA), the total RNA was extracted at different harvesting time points (0, 3, 6, and 9 h pi). The extracted RNA was subjected to reverse transcription reaction using Moloney murine leukemia virus (M-MLV) reverse transcriptase to generate cDNA, followed by qPCR analysis using SYBR Green PCR Master (Protech Technology Enterprise) and StepOne plus RT-qPCR (Applied Biosystem, Foster city, CA) instruments and their software for RNA content analysis comparisons. Primers used: (Detecting Whole RNA) matrix protein 1 (M1)-Forward primer: 5'-GAC CAA TCC TGT CAC CTC-3'; M1-Reverse primer: 5'-GAT CTC CGT TCC CAT TAA GAG-3'.[35]

Western immunoblotting assay

MDCK cells (5×10^5 cells /well) were cultured into a six-well tissue culture plate for 16–24 h under 5% CO_2, 37°C incubation. The cells were washed with DPBS once and then infected with A/WSN/33 virus (MOI = 0.1) After infection, the cells were washed with DPBS twice. Then, drug treatment (with or without **1**) was performed in E0 medium, and the cells were harvested at the indicated times. The cells were washed again with DPBS buffer, and an appropriate amount

of lysis buffer [150 mM NaCl, 1% Triton X-100 (Plusone), 0.5% sodium deoxycholate (Sigma Aldrich, New Zealand), 2 mM ethylene diamine tetraacetic acid (Amresco Inc), 50 mM Tris-HCL (pH 7.5), and 50× protease inhibitors (Roche, Germany)]. Then, the cells were scraped and collected into Eppendorf tubes and kept for 30 min on ice. The supernatant was collected by centrifugation at 14,000 *g* at 4°C for 10 min, and the protein concentration was quantified by using a Bio-Rad protein assay kit (Bio-Rad USA). An equal concentration of protein was mixed with 3X sodium dodecyl sulfate (SDS) sample buffer and heated with boiling water for 10 min, and the protein was separated by SDS polyacrylamide gel electrophoresis (SDS-PAGE). The protein on SDS-PAGE was transferred onto polyvinylidene difluoride (PVDF) membranes for western immunoblotting analysis. The antibodies used in the western blotting method were GAPDH (sc-25778; Santa Cruz Biotechnology, Inc, Santa Cruz, CA), M1 (Cat# 1321; ViroStat, Portland, ME), NP (Abcam, 20343), NS1 (Genetex, GTX125990), NS2 (Genetex, GTX125952), and PA (Genetex, GTX125932).[35]

Indirect immunofluorescence assay

MDCK cells (2×10^5 cells/well) were cultivated on coverslips in a 12-well plate and placed in a 37°C incubator with 5% CO_2 for 16 h. After the cells grew into a single layer, the culture solution was removed, washed once with DPBS, and infected with influenza virus (MOI = 0.1) for 1 h. The virus solution was removed and washed with DPBS. Then, **1** (10 μM) or **4** (1 μM) or LMB (10 nM) was added in E0, and after pi = 9 h, the supernatant was removed, washed with DPBS again, and 4% paraformaldehyde was added for 1 h to fix the cells. The following primary antibodies were used for immunofluorescence microscopy: M1 (1:50) (GTX-125928), NP (1:50) (Abcam-128193), NS2 (1:50) (GTX-125952), PA (1:50) (GTX-125932), and secondary

antibodies (Alexa Fluor-488). The nuclei were stained with 4,6-diamidino-2-phenylindole. The staining was observed by using a LSM510 microscope with a 63X oil-immersion objective lens. LMB (Sigma, MFCD-06795848) was used as the control group.[35]

Molecular docking study

To investigate the interaction of itaconic acid derivatives into the LMB binding site of CRM1, we performed a docking study by using the Libdock program of Discovery Studio Visualizer 2016 (Biovia, Corp. CA, USA). The 3D chemical structures were drawn by using Chem 3D Professional 15.0 software (PerkinElmer Informatics, Inc. CA, USA). Ligand energy minimization was performed by using an RMS gradient tolerance of 0.01. The crystal structure of CRM1 inhibitor leptomycin B in complex with CRM1-Ran-RanBP1 (PDB ID: 4HAT) was downloaded from the RCSB protein data bank and imported into the Discovery Studio Visualizer 2016 and then to the working environment of Libdock. The protein was processed by removing crystal water and other hetero atoms and adding hydrogen. The prepared protein was then used to define the binding site from the active site of LMB for docking of all prepared ligands (**1**, **4**, **6**, and **8**), including LMB, by using Libdock. Based on the highest Libdock score of the docking pose of LMB, all compounds and their interactions with CRM1 were analyzed.

SUPPORTING INFORMATION

This supporting material is available free of charge via the Internet at http://pubs.acs.org.

HPLC purity analysis data; ^{1}H and ^{13}C NMR spectra of all target compounds; 2D-interaction diagram of compounds **1** and **6** in the LMB binding site of CRM1; immunofluorescence staining to assess the effect of compound **1** on NS2, PA, and M1 protein data; and mechanism of action

of compound **4** determined by TOA assay, HAI assay, and immunofluorescence staining of M1 data were enclosed as supporting files. For the CRM1-Ran-RanBP1 (4HAT) model in complex with docking poses of compounds **1** (PDB), **4** (PDB), **6** (PDB), **8** (PDB), and LMB (PDB), the authors will release the PDB-formatted atomic coordinates and experimental data upon article publication.

Molecular formula strings with activity data (CSV).

AUTHOR INFORMATION

Corresponding Author

*P.W.H.: Phone: +886-3-2118800, ext. 3105, E-mail: pewehs@mail.cgu.edu.tw

*J.T.H.: Phone: +886-3-2118800 ext.5156, Email: jimtong@mail.cgu.edu.tw

AUTHOR CONTRIBUTIONS

B.S. performed the research, designed, synthesized, analyzed data, and wrote the manuscript. P.Y.H., Y.L.C. and C.Y.L. performed the mechanistic experiments, analyzed data. S.N.T. measured antiviral activity tests. C.F.H., T.J.L. designed and analyzed data. J.T.H and P.W.H. designed the research, analyzed data and wrote the manuscript.

The authors declare no competing financial interest.

ACKNOWLEDGEMENTS

We are very grateful for the support of this work by the grant from the Chang Gung Memorial Hospital and Chang Gung University (CMRPD1F0561-2 and BMRPB23 to P.-W. Hsieh and CMRPD1E0041-3, CMRPD1G0301-3, and BMRP416 to J.-T. Horng). The Ministry of Science and Technology of Taiwan (106-2320-B-182-004-MY3, and 106-2632-B-182-001) and the

Research Center for Emerging Viral Infections from The Featured Areas Research Center Program within the framework of the Higher Education Sprout Project by the Ministry of Education in Taiwan (MOST 107-3017-F-182-001) to J.-T. Horng. The founders had no role in the study design, the data collection and analysis, the decision to publish, or the preparation of the manuscript.

ABBREVIATIONS USED

CPE, cytopathic effect; CRM1, chromosomal region maintenance 1; HA, hemagglutinin protein; IAV, influenza A virus; IF, immunofluorescence; LMB, leptomycin B; MDCK, Madin-Darby canine kidney cells; MOI, multiplicity of infection; NEI, nuclear export inhibitor; NP, nucleoprotein; NS1, non-structural protein 1; NS2, non-structural protein 2; PA, polymerase acidic protein; RBC, red blood cell; pi, post infection; RD, rhabdomyosarcoma cells; SAR, structure-activity relationship; SI, selective index; TOA, time-of-addition; vRNP, viral ribonucleoprotein complex.

REFERENCES

1. Khanna, M.; Kumar, P.; Choudhary, K.; Kumar, B.; Vijayan, V. K. Emerging influenza virus: a global threat. *J. Biosci.* **2008**, *33*, 475-482.
2. Patel, K. K.; Patel, A. K.; Shah, S.; Ranjan, R.; Shah, S.V. Adult patient with novel H1N1 infection presented with encephalitis, rhabdomyolysis, pneumonia and polyneuropathy. *J. Glob. Infect. Dis.* **2012**, *4*, 178-181.
3. Kilbourne, E. D. Influenza pandemics of the 20th century. *Emerg. Infect. Dis*. **2006**, *12*(1), 9-14.

4. Al Hajjar, S.; McIntosh, K. The first influenza pandemic of the 21st century. *Ann. Saudi Med*. **2010**, *30*, 1-10.

5. Iuliano, A. D.; Roguski, K. M.; Chang, H. H.; Muscatello, D. J.; Palekar, R.; Tempia, S.; Cohen, C.; Gran, J. M.; Schanzer, D.; Cowling, B. J.; Wu, P.; Kyncl, J.; Ang, L. W.; Park, M.; Redlberger-Fritz, M.; Yu, H. Espenhain, L.; Krishnan, A.; Emukule, G.; van Asten, L.; da Silva, S. P.; Aungkulanon, S.; Buchholz, U.; Widdowson, M. A.; Bresee, J. S. Estimates of global seasonal influenza-associated respiratory mortality: a modelling study. *Lancet*. **2018**, *391*, 1285-1300.

6. Leiva, R.; Barniol-Xicota, M.; Codony, S.; Ginex, T.; Vanderlinden, E.; Montes, M.; Caffrey M.; Luque, F. J.; Naesens, L.; Vázquez, S. Aniline-based inhibitors of influenza H1N1 virus acting on hemagglutinin-mediated fusion. *J. Med. Chem*. **2018**, *61*, 98-118.

7. Wu, X.; Wu, X.; Sun, Q.; Zhang, C.; Yang, S.; Li, L.; Jia, Z. Progress of small molecular inhibitors in the development of anti-influenza virus agents. *Theranostics*. **2017**, *7*, 826-845.

8. Massari, S.; Goracci, L.; Desantis, J.; Tabarrini, O. Polymerase acidic protein-basic protein 1 (PA-PB1) protein-protein interaction as a target for next-generation anti-influenza therapeutics. *J. Med. Chem*. **2016**, *59*, 7699-7718.

9. Hayden, F. Developing new antiviral agents for influenza treatment: what does the future hold?. *Clin. Infect. Dis.* **2009**, *48*(Supplement_1), S3-S13.

10. Shen, Z.; Lou, K.; Wang, W. New small-molecule drug design strategies for fighting resistant influenza A. *Acta Pharm. Sin. B*. **2015**, *5*, 419-430.

11. Dilly, S.; Fotso, A. F.; Lejal, N. Zedda, G.; Chebbo, M.; Rahman, F.; Companys, S.; Bertrand, H. C.; Vidic, J., Noiray, M.; Alessi, M.; Tarus, B.; Quideau, S.; Riteau, B.;

Slama-Schwok, A. From naproxen repurposing to naproxen analogues and their antiviral activity against influenza A virus. *J. Med. Chem*. **2018**, *61*, 7202-7217.

12. World Health Organization, WHO Guidelines on the use of Vaccines and Antivirals during Influenza Pandemics. Geneva, **2004**.
13. Allen, U. D.; Aoki, F. Y.; Stiver, H. G. The use of antiviral drugs for influenza: recommended guidelines for practitioners. *Can. J. Infect. Dis. Med. Microbiol.* **2006**, *17*, 273-284.
14. Govorkova, E. A.; Webster, R. G. Combination chemotherapy for influenza. *Viruses*. **2010**, *2*, 1510-1529.
15. Hussain, M.; Galvin, H. D.; Haw, T. Y.; Nutsford, A. N.; Husain, M. Drug resistance in influenza A virus: the epidemiology and management. *Infect. Drug Resist.* **2017**, *10*, 121-134.
16. Shao, W.; Li, X.; Goraya, M. U.; Wang, S.; Chen, J. L.; Evolution of influenza a virus by mutation and re-assortment. *Int. J. Mol. Sci.* **2017**, *18*, 1650-1663.
17. Fiore, A. E.; Fry, A.; Shay, D.; Gubareva, L.; Bresee, J. S.; Uyeki, T. M.; Centers for Disease Control and Prevention (CDC). Antiviral agents for the treatment and chemoprophylaxis of influenza—recommendations of the Advisory Committee on Immunization Practices (ACIP). *MMWR Recomm Rep*. **2011**, *60*, 1-24.
18. Mai-Phuong, H. V.; Thach, N. C.; Hang, N. L. K.; Phuong, N. T. K.; Mai L. Q. Oseltamivir resistance among influenza viruses: surveillance in northern Viet Nam, 2009–2012. *Western Pac Surveill Response J*. **2013**, *4*, 25-29.
19. Perwitasari, O.; Johnson, S.; Yan, X.; Howerth, E.; Shacham, S.; Landesman, Y.; Baloglu, E.; McCauley, D.; Tamir, S.; Tompkins, S. M.; Tripp, R. A. Verdinexor, a novel selective

inhibitor of nuclear export, reduces influenza A virus replication *in vitro* and *in vivo*. *J. Virol*. **2014**, *88*, 10228-10243.

20. Pickens, J. A.; Tripp, R. A. Verdinexor targeting of CRM1 is a promising therapeutic approach against RSV and influenza viruses. *Viruses* **2018**, *10*, 48.
21. Mathew, C.; Ghildyal, R. CRM1 inhibitors for antiviral therapy. *Front. Microbiol*. **2017**, *8*, 1171-1191.
22. Xu, D.; Grishin, N. V.; Chook, Y. M. NESdb: a database of NES-containing CRM1 cargoes. *Mol. Biol. Cell*, **2012**, *23*, 3673-3676.
23. Nguyen, K. T.; Holloway, M. P.; Altura, R. A. The CRM1 nuclear export protein in normal development and disease. *Int. J. Biochem. Mol. Biol.* **2012**, *3*, 137-151.
24. Pemberton, L. F.; Blobel, G.; Rosenblum, J. S.; Transport routes through the nuclear pore complex. *Cur. Opin. Cell Biol.* **1998**, *10*, 392-399.
25. Le Sage, V.; Mouland, A. J.; Viral subversion of the nuclear pore complex. *Viruses*, **2013**, *5*, 2019-2042.
26. Kudo, N.; Matsumori, N.; Taoka, H.; Fujiwara, D.; Schreiner, E. P.; Wolff, B.; Yoshida, M.; Horinouchi, S. Leptomycin B inactivates CRM1/exportin 1 by covalent modification at a cysteine residue in the central conserved region. *Proc. Natl. Acad. Sci.* **1999**, *96*, 9112-9117.
27. Sun, Q.; Carrasco, Y. P.; Hu, Y.; Guo, X.; Mirzaei, H.; MacMillan, J.; Chook, Y. M. Nuclear export inhibition through covalent conjugation and hydrolysis of Leptomycin B by CRM1. *Proc. Natl. Acad. Sci.* **2013**, *110*(4), 1303-1308.
28. Gillis, E. P.; Eastman, K. J.; Hill, M. D.; Donnelly, D. J.; Meanwell, N. A. Applications of fluorine in medicinal chemistry. *J. Med. Chem.* **2015**, *58*, 8315-8359.

29. Mishra, S. K.; Suryaprakash, N. Intramolecular hydrogen bonding involving organic fluorine: NMR investigations corroborated by DFT-based theoretical calculations. *Molecules*, **2017**, *22*(3), 423-467.

30. Zhao, X.; Li, R.; Zhou, Y.; Xiao, M.; Ma, C.; Yang, Z.; Zeng, S.; Du, Q.; Yang, C.; Jiang, H.; Hu, Y.; Wang, K.; Mok, C. K. P.; Sun, P.; Dong, J.; Cui, W.; Wang, J.; Tu, Y.; Yang, Z.; Hu, W. Discovery of highly potent pinanamine-based inhibitors against amantadine- and oseltamivir-resistant influenza A viruses. *J. Med. Chem*. **2018**, *61*, 5187-5198.

31. Watanabe, K.; Takizawa, N.; Katoh, M.; Hoshida, K.; Kobayashi, N.; Nagata, K. Inhibition of nuclear export of ribonucleoprotein complexes of influenza virus by leptomycin B. *Virus Res*. **2001**, *77*, 31-42.

32. Hsu, J. T. A.; Yeh, J. Y.; Lin, T. J.; Li, M. L.; Wu, M. S.; Hsieh, C. F.; Chou, Y. C.; Tang, W. F.; Lau, K. S.; Hung, H. C.; Fang, M. Y.; Ko, S. Hsieh, H. P.; Horng, J. T. Identification of BPR3P0128 as an inhibitor of cap-snatching activities of influenza virus. *Antimicrob. Agents Chemother.* **2012**, *56*, 647-657.

33. Hsieh, C. F.; Chen, Y. L.; Lin, C. F.; Ho, J. Y.; Huang, C. H.; Chiu, C. H.; Hsieh, P. W.; Horng, J. T. An extract from *Taxodium distichum* targets hemagglutinin-and neuraminidase-related activities of influenza virus in vitro. *Sci. Rep.* **2016**, *6*, 36015-36028.

34. Hsieh, C. F.; Lo, C. W.; Liu, C. H.; Lin, S.; Yen, H. R.; Lin, T. Y.; Horng, J. T. Mechanism by which ma-xing-shi-gan-tang inhibits the entry of influenza virus. *J. Ethnopharmacol.* **2012**, *143*, 57-67.

35. Hsieh, C. F.; Yen, H. R.; Liu, C. H.; Lin, S. Horng, J. T. Ching-fang-pai-tu-san inhibits the release of influenza virus. *J. Ethnopharmacol.* **2012**, *144*, 533-544.

Figures

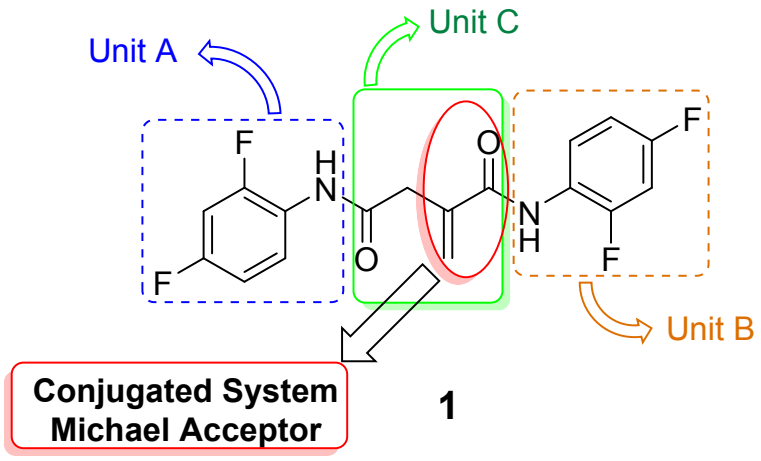

Figure 1: Lead compound **1** with its structural units.

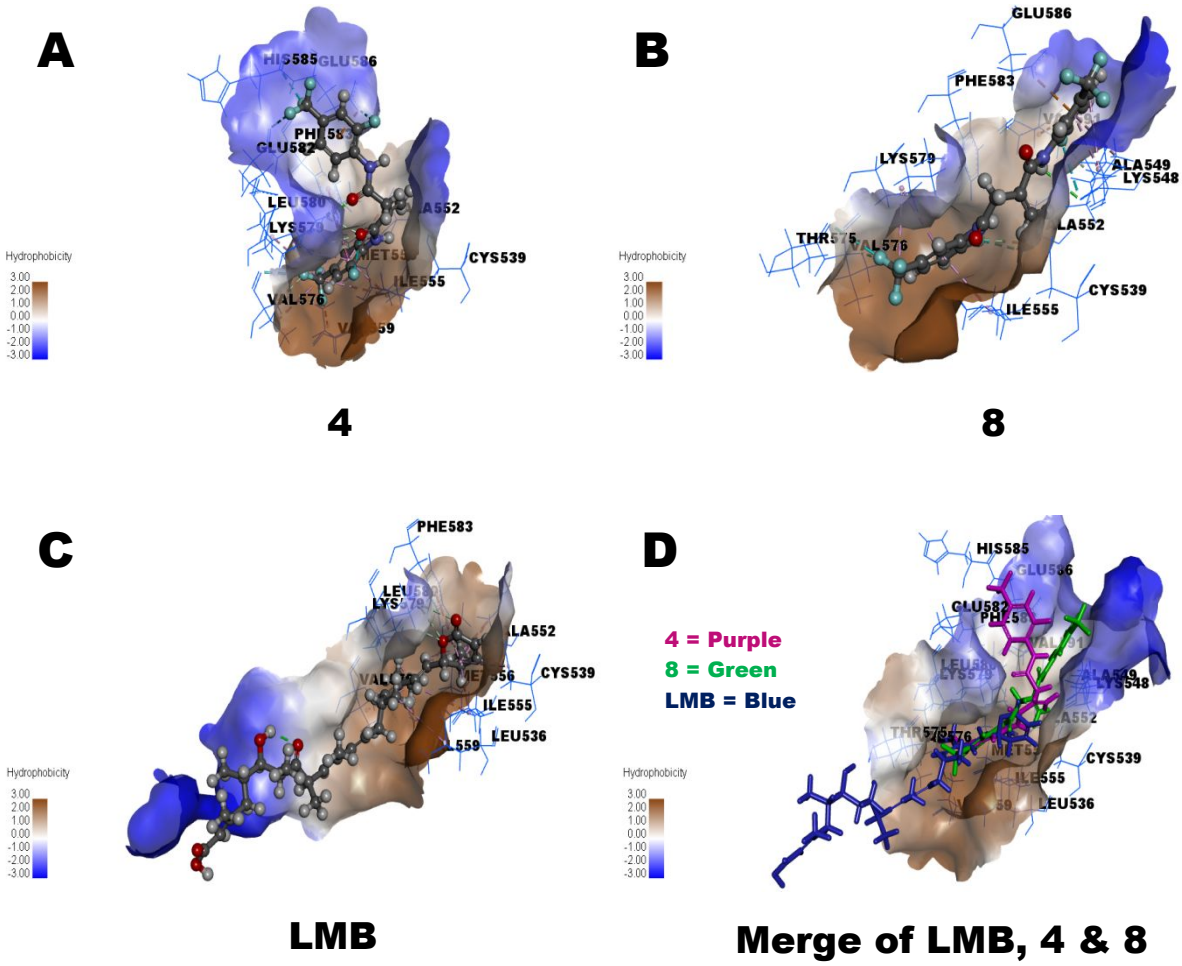

Figure 2: Molecular docking of interaction between inhibitors 4 & 8 and CRM1 in the binding sites of LMB. (A) **4**-CRM1 complex; (B) **8**-CRM1 complex; (C) LMB-CRM1 complex; and (D) the merge of **4** (purple) and **8** (green) with LMB (blue) in the binding groove of LMB in CRM1 (PDB ID: 4HAT).

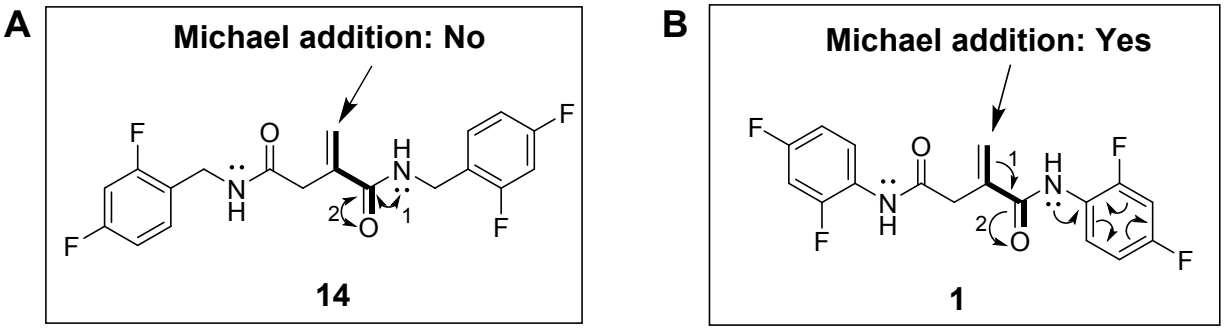

Figure 3: Compounds **14** and **1** with its Michael addition characteristics.

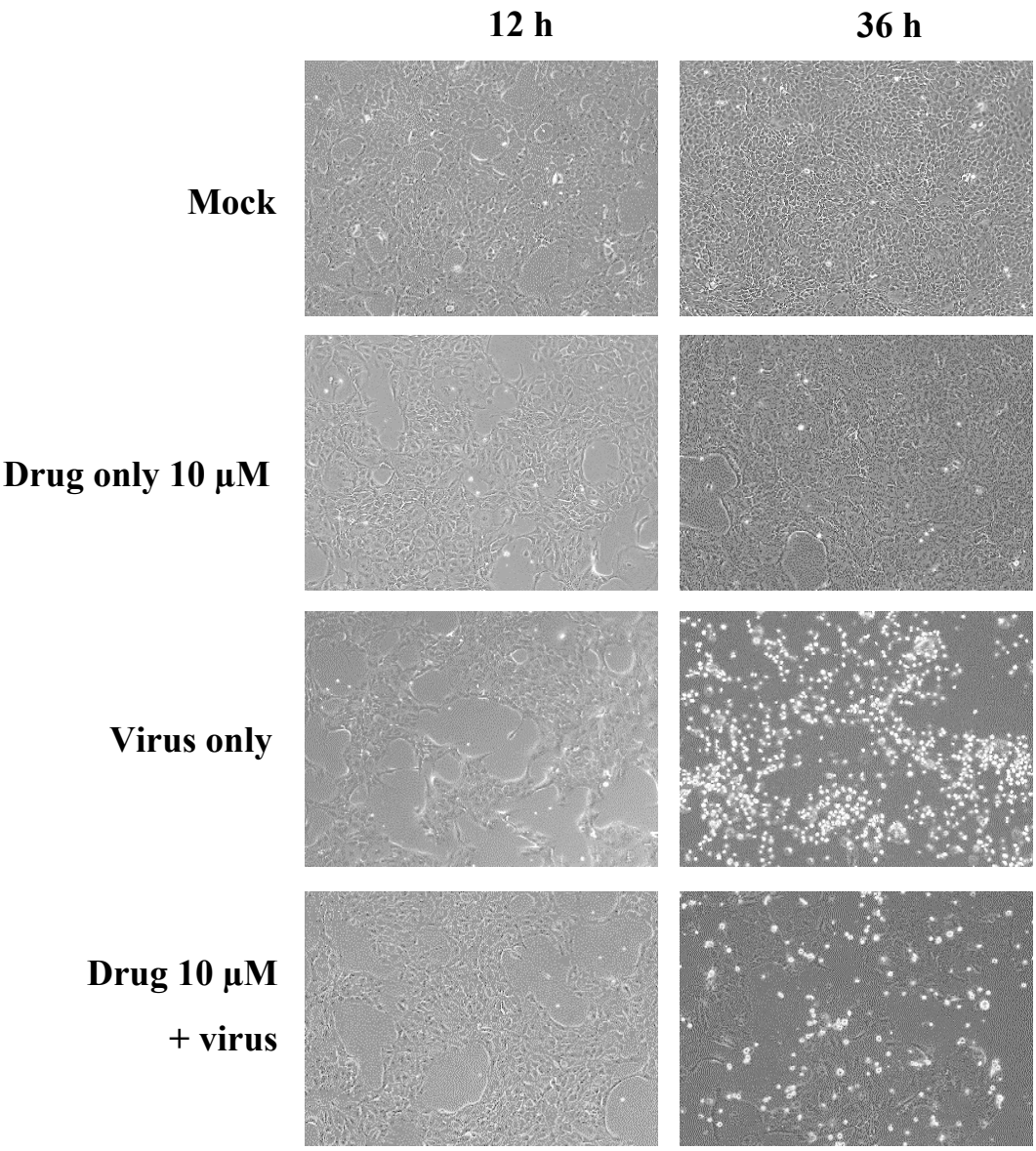

Figure 4: Compound 1 alleviates cytopathic changes induced by influenza A/WSN/33. MDCK cells were infected with A/WSN/33 influenza virus strain, with an MOI = 0.5 for 1 hour, washed with PBS, and then incubated with 10 µM of **1** in E0 medium. At pi of 12 and 36 h, the cytopathic phenomenon was recorded by observation using a microscope (Zeiss Axiovert 200M, 20x objective). The experiment was performed in three repetitions.

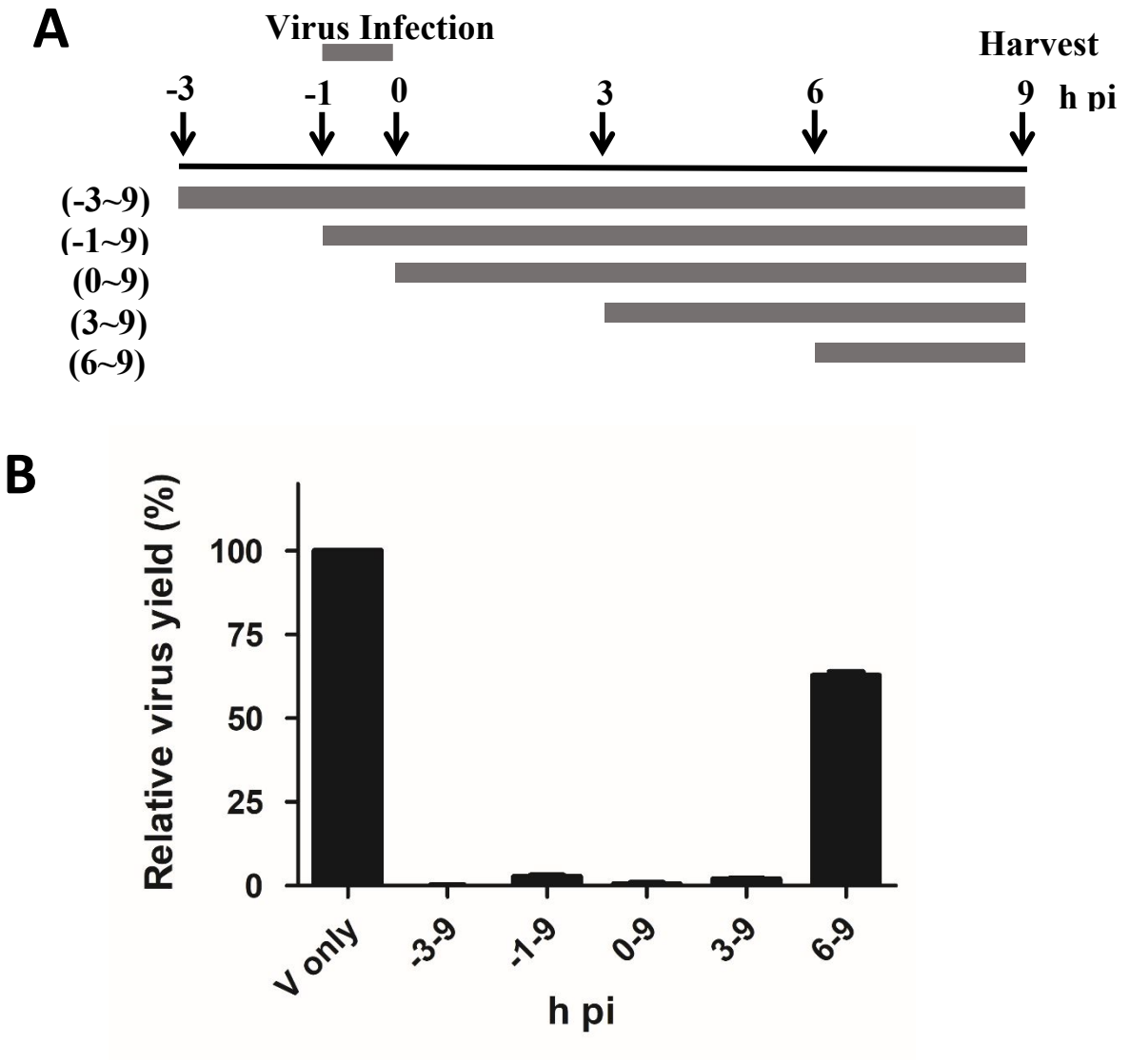

Figure 5: Time-of-addition assay to identify the step of viral life cycle targeted by 1 on influenza A/WSN/33 in MDCK cells. (A) Infection of MDCK cells with an MOI = 0.1 A/WSN/33 virus strain, and the virus adsorption time is −1 to 0 h. Compound **1** (10 μM) was added at the following periods: −3 to 9 h pi, −1 to 9 h pi, 0 to 9 h pi, 3 to 9 h pi, and 6 to 9 h pi. The supernatant was collected after 9 h pi, and the remaining viral titers were determined by plaque test. (B) The results quantification was normalized with virus only (arbitrarily set as 100%), and the experimental results are the averages from three independent experiments.

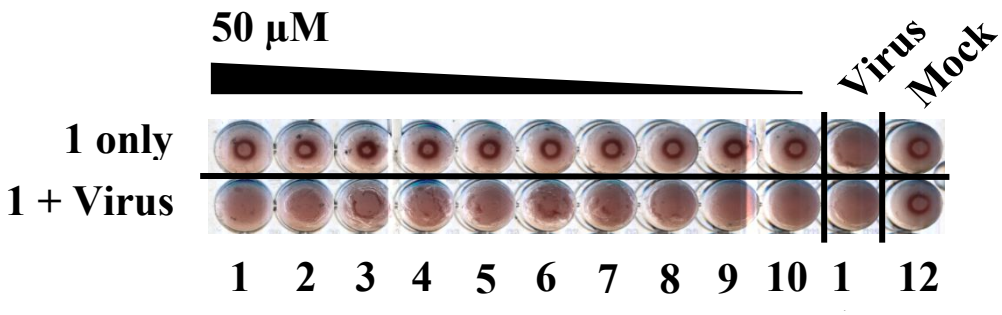

Figure 6: Effect of 1 on the HA by hemagglutination inhibition assay. The guinea pig red blood cells (RBCs) were incubated with influenza A/WSN/33 at 4 × HA on ice for 1 h with various concentrations of **1** (two-fold serial dilution from 50 μM). The RBCs precipitate at the bottom in the control group when RBCs are mixed with DMSO (lane 12), whereas the RBCs appear foggy in the virus-only group (lane 11). This result is from one of three independent experiments.

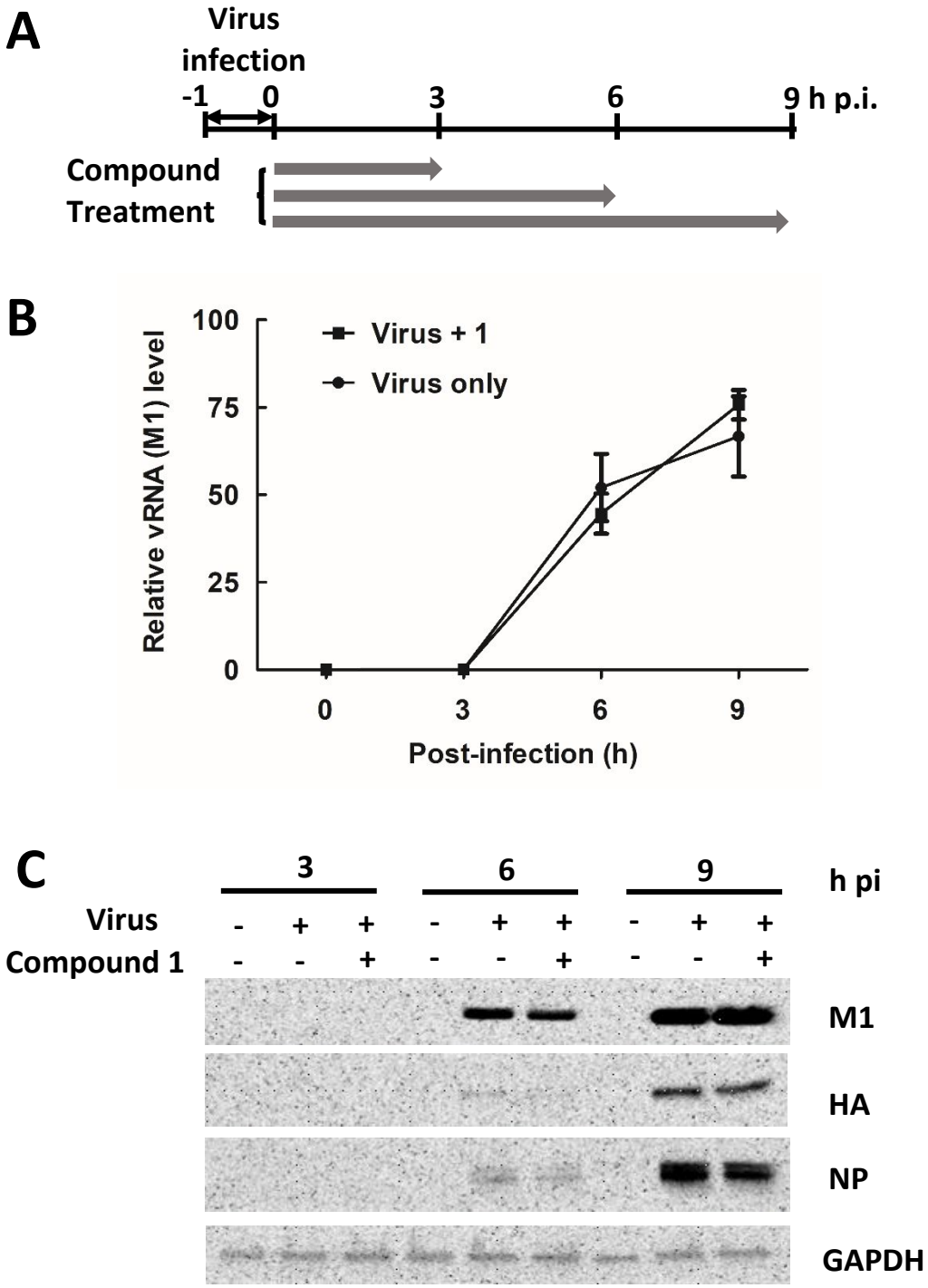
A
Virus infection
-1
0
3
6
9 h p.i.
Compound Treatment
B
Relative vRNA (M1) level
100
75
50
25
0
Virus + 1
Virus only
0
3
6
9
Post-infection (h)
C
3
6
9
h pi
Virus
Compound 1
M1
HA
NP
GAPDH

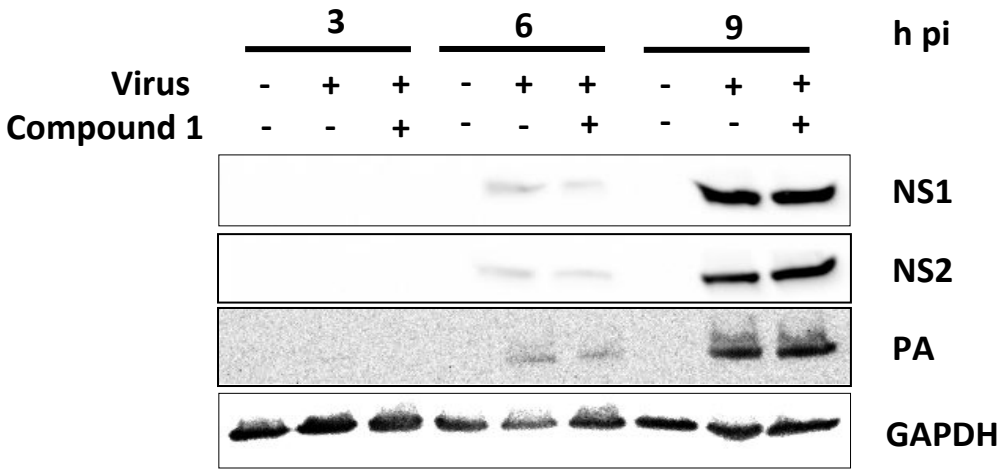

Figure 7: Exploration of post-adsorption test by vRNA inhibition assay using compound 1 treatment. (A) Design of compound **1** treatment profile. **1** (10 μM) was added to MDCK cells during or after infection at an MOI = 0.1 by A/WSN/33 strain. (B) Total RNA was extracted at the indicated time (h pi = 0, 3, 6, and 9) by using TRIzol (Invitrogen, Carlsbad, CA). An M1-specific primer was used to measure the vRNA level by RT-qPCR. GAPDH was used to prepare quantitative standards. This experiment is from one of three independent experiments. (C) Time-course protein synthesis using western blot immunoblotting analysis with antibodies against different viral proteins at 9 h pi of cell lysates.

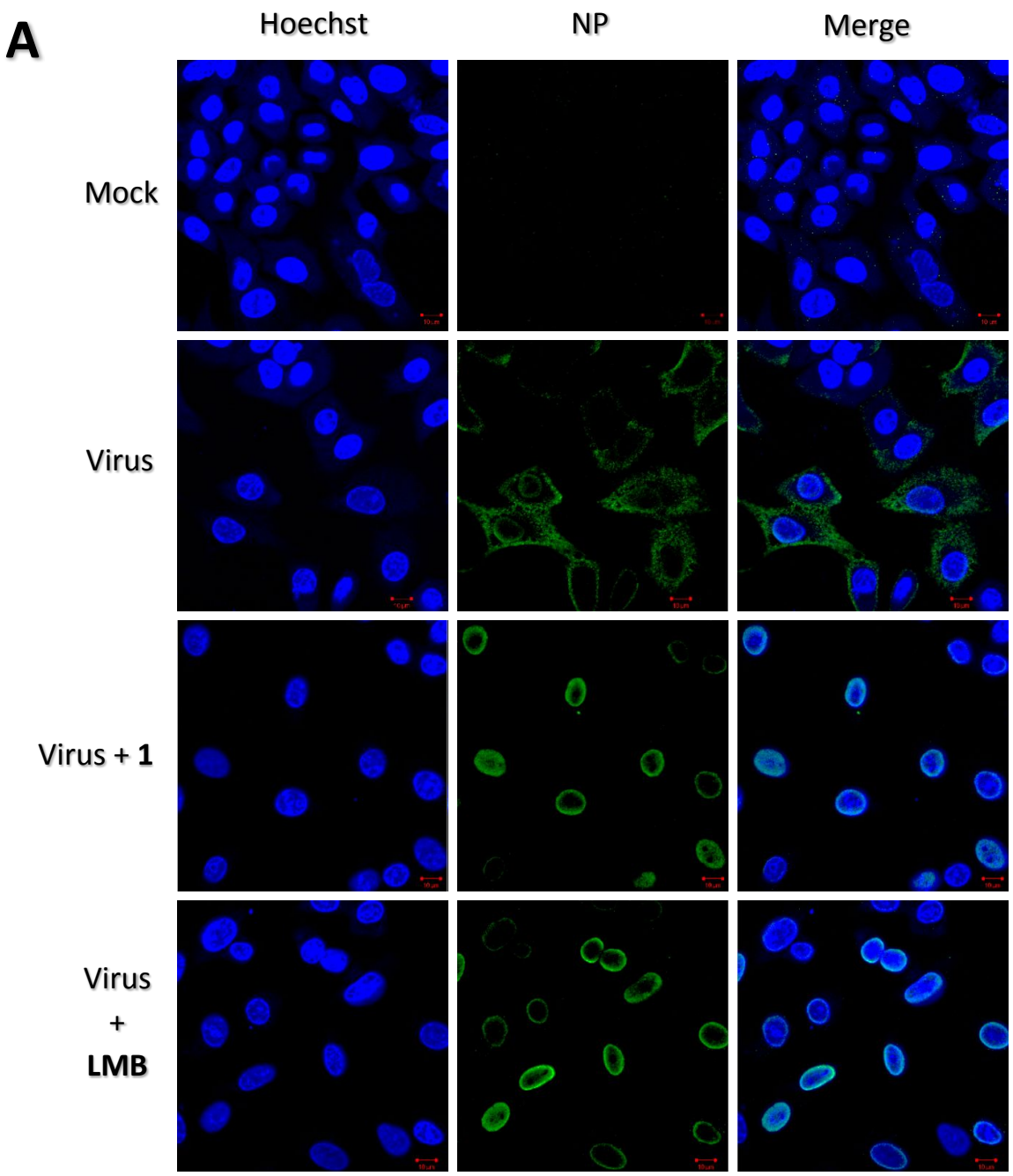
A
Hoechst
NP
Merge
Mock
Virus
Virus + 1
Virus
+
LMB

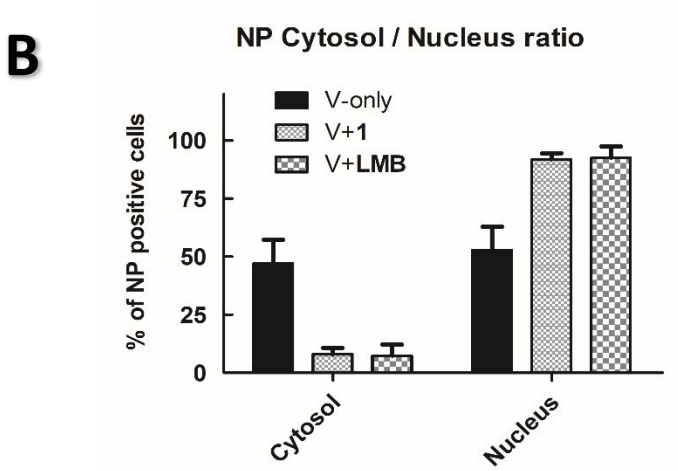

Figure 8: Detection by immunofluorescence staining of the distribution of influenza virus proteins NP by treatment with compound 1. (A) One hour after infection of MDCK cells with an MOI = 0.1 A/WSN/33 strain, 10 μM of **1** was added, and after 9 h of infection, it was fixed with 4% paraformaldehyde and immunostained with respective primary antibodies against NP (1:50). The secondary antibody used Alexa Fluor® 488, and the nuclei were stained with Hoechst. The influenza virus protein distribution was observed under a confocal microscope LSM 510 with a 63X objective. (B) ImageJ Plugins was used to quantify the intensity of the ratio of nuclear/cytoplasm distribution of NP viral protein. This experiment was verified by three independent experiments.

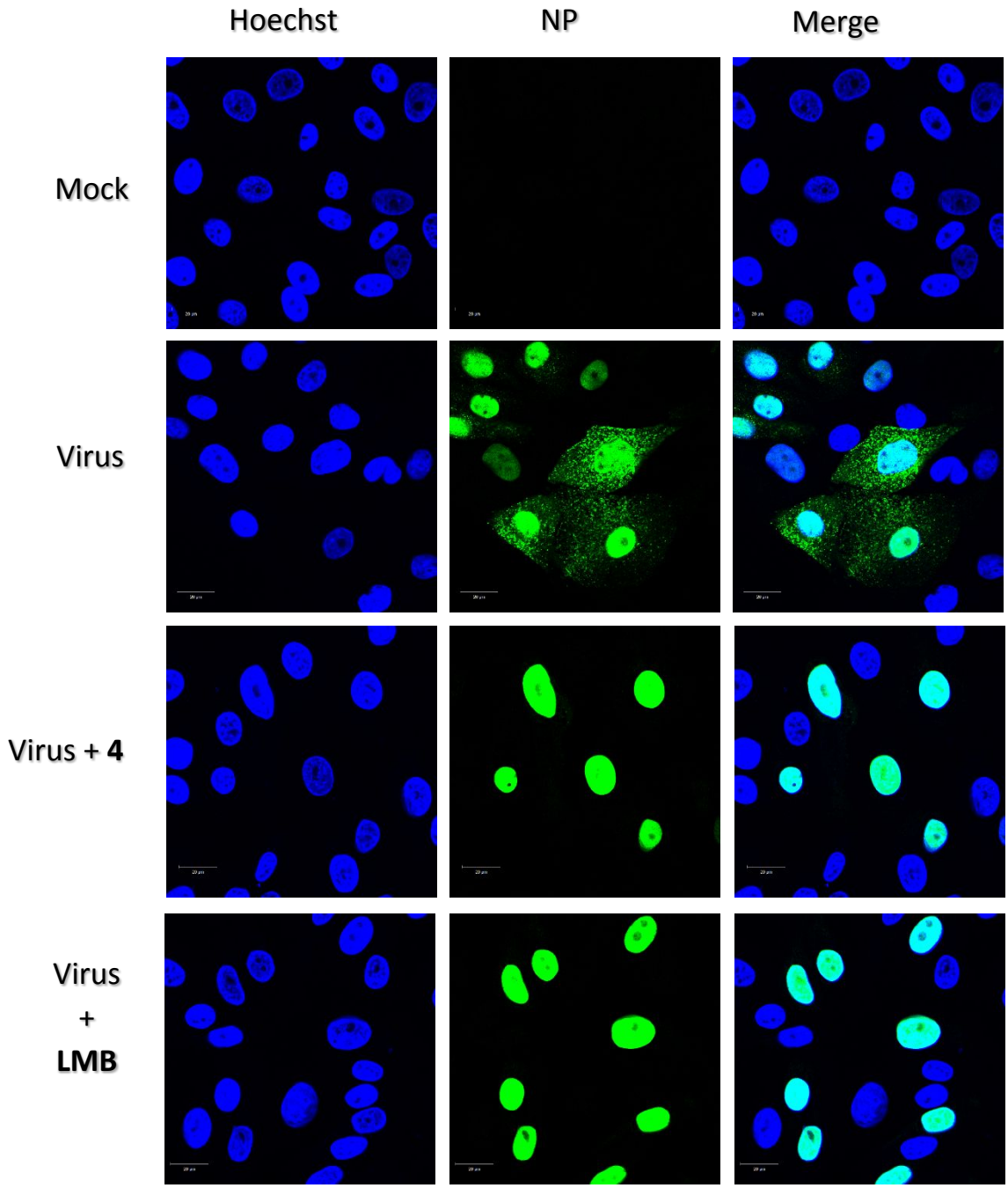

Figure 9: Detection by immunofluorescence staining of the distribution of influenza virus proteins NP by treatment with compound 4. One hour after infection of MDCK cells with an MOI = 0.1 of A/WSN/33 strain, 1 µM of **4** was added, and after 9 h of infection, it was fixed with 4% paraformaldehyde and immunostained with respective primary antibodies against NP (1:50). The secondary antibody used Alexa Fluor® 488, and the nuclei were stained with Hoechst.

Influenza virus protein distribution was observed under a confocal microscope LSM 510 with a 63X objective. LMB was used as a positive control. Two independent experiments were performed for verification.

Schemes

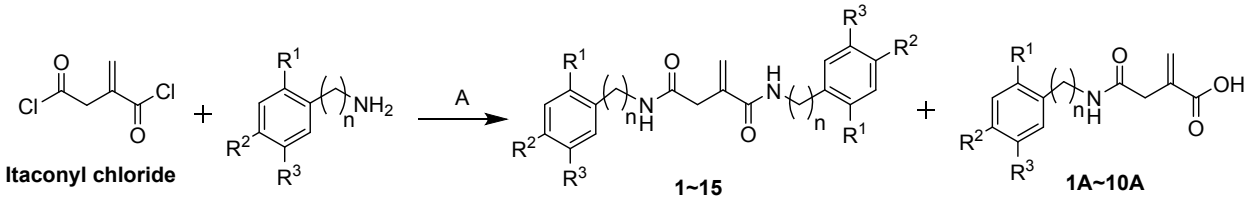

Scheme 1: Reaction conditions and reagents (A) Dry DCM, Molecular sieve (MS), −4 to 0°C for 1 h, rt for 4 h to 1 d (TLC confirmation necessary).

Tables

Table 1: *In-vitro* anti-influenza A virus activities of the itaconic acid derivatives (1~15).

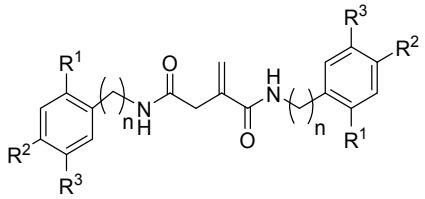

Compounds	R^1	R^2	R^3	n	NH signals	EC_{50} (μM)	CC_{50} (μM)	SI
1	F	F	H	0	8.73, 8.21	2.84 ± 0.31	84.72 ± 4.41	29.83
2	F	Cl	H	0	8.75, 8.18	0.67 ± 0.04	>110	>164
3	F	Br	H	0	8.77, 8.18	0.99 ± 0.11	>110	>111
4	F	CF_3	H	0	8.92, 8.32	0.14 ± 0.04	>110	>785
5	F	$-OCH_3$	H	0	8.60, 8.12	31.04 ± 0.66	>110	>3
6	F	H	F	0	8.82, 8.24	1.26 ± 0.03	32.77 ± 2.46	26.01
7	F	H	Cl	0	8.73, 8.21	0.18 ± 0.12	19.91 ± 0.30	110.61
8	F	H	CF_3	0	8.82, 8.30	0.11 ± 0.03	14.97 ± 1.97	136.09
9	F	H	$-OCH_3$	0	8.72, 8.23	0.48 ± 0.02	>110	>229
10	Br	F	H	0	8.51, 8.27	2.59 ± 0.20	>110	>42
11	CF_3	F	H	0	8.50, 8.10	>50	>110	ND
12	CF_3	H	H	0	8.55, 8.20	>50	>110	ND
13	Br	Br	H	0	8.56, 8.34	41.56 ± 2.15	>110	>2
14	F	F	H	1	7.00, 7.00	>50	>110	ND
15	F	H	F	1	6.98, 6.85	>50	>110	ND
LMB	-	-	-	-	-	0.18 ± 0.02	>0.88	>4
Verdinexor	-	-	-	-	-	3.28 ± 0.21	31.77 ± 2.40	9.69

Effective concentration for 50% inhibition (EC_{50}) in μM; cytotoxicity concentration for 50% cell death (CC_{50}) in μM; selectivity index (SI) calculated as the ratio of CC_{50} to EC_{50}; data represent the mean ± S.D. ($n \geq 3$), ND: not determined; leptomycin B (LMB) and verdinexor used as positive controls.

Table 2: *In-vitro* anti-influenza A virus activity of the itaconic acid derivatives (1A~10A).

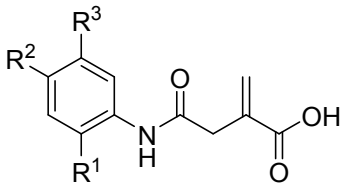

Compounds	R^1	R^2	R^3	EC_{50} (μM)	CC_{50} (μM)	SI
1A	F	F	H	>50	>110	ND
2A	F	Cl	H	>50	>110	ND
3A	F	CF_3	H	>50	>110	ND
4A	F	H	F	>50	>110	ND
5A	F	H	CF_3	>50	>110	ND
6A	F	F	Cl	>50	>110	ND
7A	CF_3	F	H	>50	>110	ND
8A	CF_3	H	F	>50	>110	ND
9A	CF_3	H	H	>50	>110	ND
10A	H	H	CF_3	>50	>110	ND

Effective concentration for 50% inhibition (EC_{50}) in μM; cytotoxicity concentration for 50% cell death (CC_{50}) in μM; selectivity index (SI) calculated as the ratio of CC_{50} to EC_{50}; data represent the mean ± S.D. ($n \geq 3$); ND: not determined.

Table 3: Inhibition spectrum of 1 and 4 against different virus strains

	[a]CC_{50} (μM)			
Cells	**1**		**4**	
RD	74.60 ± 6.47		9.31 ± 0.42	
MDCK	84.72 ± 4.41		>110	
Viruses	[b]EC_{50} (μM)		[c]**SI**	
Influenza Virus	**1**	**4**	**1**	**4**
A/WSN/33 (H1N1)	2.84 ± 0.31	0.33 ± 0.02	30	>333
A/TW/90206/09 (H1N1pdm)[d]	2.98 ± 0.83	ND	28	ND
A/TW/2235/09 (H1N1pdm)[d]	2.36 ± 0.11	1.62 ± 0.07	36	>67
A/TW/7855/09 (H1N1)[e]	2.60 ± 0.12	ND	33	ND
A/TW/6663/09 (H1N1)[e]	4.83 ± 1.89	ND	18	ND
A/TW/3446/02 (H3N2)	4.60 ± 0.16	0.96 ± 0.04	18	>114
B/TW/00482/13	3.77 ± 0.03	ND	22	ND
B/TW/03384/13	3.75 ± 0.04	ND	23	ND
B/TW/00642/14	3.44 ± 0.21	ND	25	ND
B/TW/01061/14	3.97 ± 0.03	ND	21	ND
Enterovirus (EV)				
EV A71 TW/2231/1998	4.50 ± 0.91	ND	16	ND
EV A71 TW/4643/1998	ND	6.69 ± 0.27	ND	1
EV D68 TW/2795/2014 (Clade B3)	>50	>50	ND	ND
Rhinovirus				
Rhinovirus/71803	>50	>50	ND	ND

Rhinovirus/71903	>50	>50	ND	ND

[a]CC_{50} was determined by MTT assay; [b]EC_{50} was determined by neutralization assay using crystal violet staining, MDCK cells were used for influenza viruses, RD cells were used for enterovirus and rhinovirus; [c]Selectivity index (SI) calculated as the ratio of CC_{50} to EC_{50}; [d]Pandemic H1N1 (SOIV) strains; [e]Strains clinically resistant to oseltamivir. Data are presented as the mean ± SDs of the results from three independent experiments. ND: not determined.

TABLE OF CONTENT GRAPHIC